Inorganic Chemistry Communications 151 (2023) 110625

Contents lists available at ScienceDirect

Inorganic Chemistry Communications

journal homepage: www.elsevier.com/locate/inoche

Short communication

Enhanced removal of anionic Methyl orange azo dye by an iron oxide (Fe_3O_4) loaded lotus leaf powder (LLP@Fe_3O_4) composite: Synthesis, characterization, kinetics, isotherms, and thermodynamic perspectives

Venkata Subbaiah Munagapati [a], Hsin-Yu Wen [b], Anjani R.K. Gollakota [c,d], Jet-Chau Wen [a,c,*], Chi-Min Shu [c], Kun-Yi Andrew Lin [e], Vijaya Yarramuthi [f], Jhy-Horng Wen [g], Guda Mallikarjuna Reddy [h,i], Grigory V. Zyryanov [i,j]

[a] Research Centre for Soil & Water Resources and Natural Disaster Prevention (SWAN), National Yunlin University of Science and Technology, Douliou, Yunlin 64002, Taiwan, ROC
[b] Department of Pathology, West China Hospital, Sichuan University, Chengdu 610041, PR China
[c] Department of Safety, Health, and Environmental Engineering, National Yunlin University of Science and Technology, Douliou, Yunlin 64002, Taiwan, ROC
[d] Department of Chemical and Materials Engineering, National Yunlin University of Science and Technology, Douliou, Yunlin 64002, Taiwan, ROC
[e] Department of Environmental Engineering, National Chung Hsing University, 250 Kuo-Kuang Road, Taichung, Taiwan, ROC
[f] Department of Chemistry, Vikrama Simhapuri University, Nellore 524324, Andhra Pradesh, India
[g] Department of Electrical Engineering, Tunghai University, Taichung 40704, Taiwan, ROC
[h] Department of Chemistry, Sri Venkateswara University, Tirupati 517502, Andhra Pradesh, India
[i] Chemical Engineering Institute, Ural Federal University, 620002 Yekaterinburg, Russian Federation
[j] Ural Division of the Russian Academy of Sciences, I. Ya. Postovskiy Institute of Organic Synthesis, 22 S. Kovalevskoy Street, Yekaterinburg, Russian Federation

ARTICLE INFO

Keywords:
Adsorption
Iron oxide
Lotus leaf powder
Magnetic separation
Regeneration
Methyl orange

ABSTRACT

The goal of this work was to prepare a novel magnetic nanocomposite of Lotus leaf powder@iron oxide (LLP@Fe_3O_4) to remove Methyl Orange (MO) from a liquid medium. The co-precipitation approach was used to successfully synthesize the LLP@Fe_3O_4 composite, which was then characterized using FT-IR, XRD, pH_{PZC}, SQUID-VSM, BJH/BET, and FE-SEM/EDX analysis. Batch tests were carried out to investigate the adsorption behaviour and mechanisms. The optimal MO removal efficiency of LLP@Fe_3O_4 reached up to 94.3% under the optimum reaction conditions (LLP@Fe_3O_4 dosage = 50 mg/30 mL, stirring speed = 200 rpm, contact period = 120 min, MO initial concentration = 20.8 mg/L, temperature = 298 K, and pH = 5.1). Adsorption isotherms and kinetics were analyzed using Temkin, Freundlich, Langmuir, Dubinin-Radushkevich (D-R), pseudo-second-order (PSO), intra-particle diffusion (IPD), pseudo-first-order (PFO), and Elovich models. Adsorption of MO on LLP@Fe_3O_4 is best matched to the Langmuir isotherm and PSO kinetic models. The data was analyzed utilizing four errors (SSE, ARE, RMSE, and χ^2) and regression coefficient functions to estimate the best-fitting kinetic and isotherm models. The maximal monolayer adsorption uptake of MO was estimated to be 282.3 mg/g at 298 K. The thermodynamic variables, namely entropy (ΔS^o = -98 J/mol K), enthalpy (ΔH^o = -35.6 kJ/mol), and Gibbs free energy (ΔG^o = -6.2808 kJ/mol at 298 K), indicated that the adsorption of MO onto LLP@Fe_3O_4 was spontaneous, exothermic, and feasible. The LLP@Fe_3O_4 composite may be regenerated and readily separated from the liquid medium without losing any weight. After regeneration, the LLP@Fe_3O_4 still has good adsorption efficiency for up to five cycles of adsorption and desorption. The experimental findings of this study output could be confirmed that LLP@Fe_3O_4 is a potential adsorbent to remove dyestuff from wastewater.

1. Introduction

In order for humans to survive and exist in the universe, water is a must. However, concerns with water contamination brought on by dyes, metal ions, and antibiotics have received increased attention globally as a result of large industrial output and rapid population expansion. Especially in textile, paper mill, leather, plastic, rubber, paint,

* Corresponding author at: Research Centre for Soil & Water Resources and Natural Disaster Prevention (SWAN), National Yunlin University of Science and Technology, Douliou, Yunlin 64002, Taiwan, ROC.
E-mail address: wenjc@yuntech.edu.tw (J.-C. Wen).

https://doi.org/10.1016/j.inoche.2023.110625
Received 16 December 2022; Received in revised form 9 March 2023; Accepted 12 March 2023
Available online 16 March 2023
1387-7003/© 2023 Elsevier B.V. All rights reserved.

cosmetics, and other industries, dyes are widely employed as coloring agents [1]. Synthetic dyes and pigments are manufactured in excess of 100,000 different types and 700,000 tons yearly. Nevertheless, throughout the numerous uses and manufacturing processes, 10–15% of dyestuffs are released into the industrial effluent [2]. Disposing of dye-containing wastewater into the environment (wetlands, agricultural fields, and rivers) results in (a) risks to human health, (b) decreased crop quality and soil fertility, (c) a decrease in biodiversity due to the prevention of photosynthesis for aquatic plants, and (d) a decrease in water quality due to an increase in oxygen demand as measured by BOD (Biochemical Oxygen Demand), TOC (Total Organic Carbon), and COD (Chemical Oxygen Demand) values [3]. Thus, the treatment of industrial pollutants is critical and the need of the hour.

Methyl orange dye is one of the notable anionic/acidic dyes which leads to environmental risks. The general features of MO dye are listed in Table 1. MO dye has been extensively used in various industries, including, paper, food, textile, pharmaceutical, and other research-based laboratories. The presence of a single azo group in MO causes MO becomes resistant to undergoing biodegradation, and affects life at their genetic level (teratogenic, carcinogenic, and mutagenic aberrations) [4]. By chance, if the MO dye enters the human system, the gastrointestinal bacteria metabolize the dye into an aromatic amine, which can cause, cyanosis, quadriplegia, jaundice, vomiting, and elevated heart rate in humans [5]. Keeping in view of these deleterious effects, MO dye treatment before being disposed of in water bodies has become essential.

Nomenclature

ARE	Average relative error
A_T	Temkin constant
B_T	Constant related to the heat of sorption
BET	Brunauer-Emmett-Teller
BJH	Barrett-Joyner-Halenda
C	Constant that represents the thickness of the boundary layer
C_e	MO equilibrium concentration (mg/L)
C_{Ae}	MO concentration at equilibrium in the solid phase (mg/L)
C_o	Initial MO concentration (mg/L)
FE-SEM	Field Emission-Scanning Electron Microscopy
FT-IR	Fourier Transform Infrared
K_c	Equilibrium constant
K_f	Freundlich constant
K_L	Langmuir constant
K_{id}	IPD rate constant
k_1	PFO rate constant
k_2	PSO rate constant
M	LLP@Fe_3O_4 mass (mg)
n	Measure of the deviation from linearity of adsorption
$1/n$	Heterogeneity factor
q_e	Quantity of MO adsorbed at equilibrium (mg/g)
q_{e1}	MO uptake at equilibrium
q_{e2}	MO uptake at equilibrium
$q_{e,\exp}$	MO adsorbed amounts at equilibrium, experimental value (mg/g)
$q_{e,cal}$	MO adsorbed amounts at equilibrium, calculated value (mg/g)
q_m	D-R monolayer uptake
q_{max}	Adsorption uptake
q_t	Amount of MO adsorbed at time t (mg/g)
R	Gas constant (8.314 kJ/mol K)
RMSE	Root mean square error
SSE	Sum of square error
SQUID-VSM	Superconducting Quantum Interference Device-Vibrating Simple Magnetometer
T	Temperature (K)
V	Volume of MO (L)
XRD	X-ray Diffraction

Greek letters

β	Constant related to sorption energy
ε	Polanyi potential
α	Elovich model initial adsorption rate
β	Elovich model desorption constant
χ^2	Chi-square

Table 1
The characteristics of MO.

Property	Value
IUPAC name	Sodium-4-(4-dimethylamino phenyl diazenyl) benzenesulfonate
Molecular formula	$C_{14}H_{14}N_3SO_3Na$
Molecular weight	327.34 g/mol
pKa	3.7
Colour and form	Orange-yellow powder or crystalline scales
Melting point	>300 °C
Solubility	<1 mg/mL (18 °C)
Structure	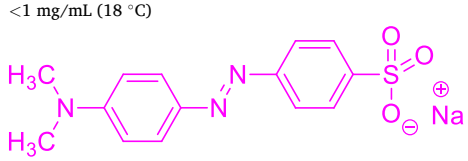

Numerous conventional techniques, including ion exchange [6], reverse osmosis [7], coagulation/flocculation [8], photocatalytic degradation [9–11], ultrafiltration membrane [12], incineration [13], solvent extraction [14], adsorption [15–24], and so on, have been utilized effectively for harmful pollutant treatment. The advantages and disadvantages of these conventional techniques are given in Table 2. Adsorption is one of the most chosen processes because of its features such as high flexibility, ease of application, high efficiency, simplicity of design, cheap cost, environmental benignity, and plenty of adsorbents. Activated carbon, activated diatomite, resin, carbon aerogel, carbon nanotubes, clays/zeolites, polymers, graphene oxide, and other porous materials have been used in the adsorption technique to remove contaminants from wastewater [25–27]. The problem with these materials is that either their precursors are expensive or their synthetic routes require lengthy and complicated reactions or require nonviable reaction conditions for scaling up. To overcome these challenges, extremely affordable, naturally accessible, and environmentally friendly adsorbents can be employed for effective water treatment.

Agricultural waste has recently been identified as a suitable adsorbent because of its low cost, vast availability, and environmental friendliness. The role of plant-based materials in the elimination of potentially toxic dyes from the aquatic system is growing. In this connection, it is worth mentioning here a perennial aquatic herb, Lotus (*Nelumbo nucifera*), which is a common farm product and an ornamental plant. The lotus leaves possess rich plant fibers, various functional groups (hydroxyl and carboxyl), and proteins [28]. In this study, Lotus leaves powder was chosen as a raw adsorbent material. Nevertheless, using lotus leaf powder as such leads to low adsorption capacity, reduced specific surface area, and also removal of the powder will be difficult after the completion of the adsorption process. Therefore,

Table 2
Advantages and disadvantages of wastewater treatment methods.

Treatment method	Advantages	Disadvantages
Ion-exchange	• Efficient and rapid process • Simple and easy to use • High capacity • Scalability • Versatility • Regenerability • Wide range of applications	• Too expensive • Limited selectivity • Chemical compatibility • Large volumes require columns • Sensitive to effluent pH • Waste generation • Fouling
Reverse osmosis	• High efficiency • East to operate • Wide range of applications • Low energy consumption	• Wastewater production • Cost • Slow water production • Dependence on electricity
Coagulation/ Flocculation	• Low-cost • Highly efficient for suspended solids and colloidal particles • Simple process • Bacterial inactivation capability	• Requires adjunction of non-reusable coagulants and flocculants • Large generation of sludge volume • Poor removal
Photocatalytic degradation	• Low capital cost • Reuse of photocatalyst • Complete degradation of pollutants • Environment friendliness	• Limited effectiveness • Catalyst deactivation • Energy consumption • Catalyst cost • Formation of secondary pollutants • Limitations on applicability
Ultrafiltration membrane	• Requires small space • Efficient, uncomplicated, and rapid process • No chemicals needed • Generate relatively less solid waste	• High energy requirements • High operation and maintenance costs • Rapid fouling on membrane • Limited flowrates
Incineration	• Volume reduction • Energy production • Waste reduction • Reduced greenhouse gas emissions	• Air pollution • High cost • Negative public perception • Limited applicability • Ash residue
Solvent extraction	• Common for wastewater recycle • Usage in large-scale activities with heavy contamination loads • Very affordable operating costs • Simple process monitoring and control	• High equipment cost • Difficult to recover solvents • Large volume of solvent needed • Use of organic solvents are highly flammable/or toxic
Adsorption	• Flexibility • Simple operation design • High efficiency • Cost-effectiveness • Environmental benignity • Plenty of adsorbents • Good recycle performance	• pH dependent • Relatively high cost of materials • Generation of waste products • Performance depends upon adsorbent

modification of lotus leave powder is essential to overcome these limitations. In this context, special emphasis was put on the use of magnetic nano adsorbents. Because of their significant super-paramagnetic activity, non-toxicity, ease of manufacture, high thermal stability, and environmental friendliness, iron oxide (Fe_3O_4) nanoparticles are one of the most often utilized materials in wastewater treatment [29]. The inclusion of magnetite Fe_3O_4 nanoparticles into agricultural waste improves surface area and reactivity while decreasing intraparticle diffusion rate and improving adsorption efficiency and reusability [30]. In general, the saturated sorbents are either filtered or centrifuged from the aqueous medium following the adsorption process, which is both time-consuming and energy-intensive. The saturated sorbents, on the other hand, may be swiftly separated and reused several times utilizing magnetic nano adsorbents. Magnetite (Fe_3O_4) displays the strongest magnetism among other iron oxides [31]. Several studies have been conducted to evaluate the use of Fe_3O_4 nanoparticle-coated biomass as adsorbents for possibly hazardous color cleanup [32–36].

In this work, a new kind of LLP@Fe_3O_4 magnetic nanocomposite was synthesized utilizing the co-precipitation process and employed for the adsorptive elimination of MO from an aqueous environment. pH_{PZC}, FTIR, FE-SEM/EDX, XRD, SQUID-VSM, and BJH-BET techniques were used to characterize LLP@Fe_3O_4. Adsorption process variables such as solution pH, LLP@Fe_3O_4 dose, contact period, agitation speed, starting MO concentration, and MO temperature were also studied. In addition, isotherm, kinetics, thermodynamics, desorption, and regeneration studies were conducted.

2. Materials and methods

2.1. Materials

Lotus leaves were gathered from the YUNTECH campus, Douliou, Taiwan. NaOH (sodium hydroxide) pellets, HCl (hydrochloric acid), KNO_3 (potassium nitrate), $FeSO_4{\cdot}7H_2O$ (ferrous sulfate heptahydrate), $FeCl_3{\cdot}6H_2O$ (ferric chloride hexahydrate), and MO dye were acquired from Sigma Aldrich (USA). The aforementioned reagents were all of the analytical quality and were utilized without any prior purification. DI (Deionized) water was prepared to exhibit conductivity of < 18 MΩ-cm.

2.2. Preparation of standard solution

1.18 g of MO was dissolved in 1000 mL of DI water to make a standard solution with a concentration of 1000 mg/L. This solution's concentration was then diluted to the appropriate amount for use in further studies.

2.3. Preparation of lotus leaf powder

The collected lotus leaves were first washed, dried, and powdered. The powder was then rinsed with DI water and dried at 70 °C for 10 h before being boiled in DI water and changed frequently until the water became colorless, indicating the elimination of the water-soluble color composites. The cleaned and boiled powder was dried in an air oven at 80 °C for 10 h. After drying, the powder was sieved using a 30-mesh sieve tray. The powder is labelled as lotus leaf powder (LLP).

2.4. Synthesis of LLP@Fe_3O_4 composite

The co-precipitation method [30] was used to make the LLP@Fe_3O_4 composite. In summary, 7.80 g of $FeCl_3{\cdot}6H_2O$ and 3.80 g of $FeSO_4{\cdot}7H_2O$ were dissolved in 400 mL of DI water. At 60 °C, the mixture was vigorously mixed for 40 min. The solution was then added 10.0 g of LLP while being constantly agitated. While stirring, a dropwise addition of sodium hydroxide (5.0 M) solution was made to raise the pH to 11.0 and precipitate metal hydroxides and afterward hydrated metal oxides [37]. During this time, the reaction mixture's colour changed to black, confirming the synthesis of iron oxide nanoparticles, LLP@Fe_3O_4. The liquid was then vigorously mixed for 1 h at 60 °C before being cooled to room temperature. An external magnetic field was then used to separate the nanocomposite precipitate from the mixture. Furthermore, the precipitate was rinsed multiple times with DI water until it reached neutral pH and dried in an oven at 70 °C for 12 h. The LLP@Fe_3O_4 was stored in an airtight glass container for characterization and batch adsorption experiments.

2.5. Instrumentation

The characteristics of the adsorbents LLP, LPP@Fe_3O_4, and MO-LPP@Fe_3O_4 were examined utilizing different instrumental techniques. The surface functional groups on the samples were examined using an

FT-IR (Thermo Nicolet iS10; USA) spectrophotometer with a resolution of 5 cm^{-1} across the wavenumber ranging from 400 to 4000 cm^{-1}. The solid samples were made as KBr (potassium bromide) pellets. Each sample was combined with around 100 mg of KBr before being exposed to a pressure of about 1400 kPa in a hydraulic press. The surface morphologies and elemental composition of the materials were investigated using an FE-SEM (JSM-7610F Plus; JEOL; Japan) connected to an EDX. Prior to the examination, the samples were mounted on metal (aluminium) stubs with double-sided carbon taps, coated with palladium/gold using a sputter coater at 20 mA, and then viewed using FE-SEM/EDX equipment at various working distances and accelerating voltage. The crystalline structures of materials were determined using an XRD (AXS D8 Advance XRD; Germany) in the 2θ range of 10.0–80.0° with Cu Kα radiation (λ = 1.54059 Å) at ambient temperature. Textural parameters such as pore radius, surface area, and pore volume of materials were evaluated from N_2 adsorption–desorption isotherms at 76 K using a pore size and surface area analyzer (Quantachrome, Autosorb IQ, USA). Prior to testing, the samples were degassed to 473 K for 240 min to remove any pollutants physically adsorbing in the pores. The magnetic property of Fe-LPP was measured using the SQUID-VSM magnetometer (Quantum Design; MPMS3; USA), with magnetic fields ranging between ± 20000 Oe. All pH measurements were taken using a Mettler Toledo Seven Easy (USA) pH meter. A UV–Vis spectrophotometer (Jasco V 750; Japan) at a wavelength of 464 nm was used to measure the concentration of MO in the solution.

The solid addition procedure was used to calculate the pH_{PZC} (point of zero charge) of the LPP@Fe_3O_4. In short, 30.0 mL of KNO_3 0.1 M electrolyte was put into a sequence of 50.0 mL glass vials, and the initial pH (pH_i) of each vial was adjusted from 1.0 to 10.0 by the addition of either 0.1 M NaOH or HCl solutions. Following the addition of 50 mg of LPP@Fe_3O_4 to each sample, the solution was stirred at 298 K for 24 h to ensure thorough contact with the sample. The final pH (pH_f) value of the filtrate was then determined. The pH (the variance between the pH_i and pH_f values) was computed, and the pH_i was plotted versus the pH. The pH_{PZC} value of the LPP@Fe_3O_4 is the junction point of the horizontal line in the graph (X-axis) at ΔpH = 0.

2.6. Adsorption experimental procedure

The following parameters were maintained for the various sets of batch tests:

- Influence of pH was examined in the pH range from 1.06 to 10.2, LLP@Fe_3O_4 dosage 50.0 mg, solution volume 30.0 mL, concentration 20.8 mg/g, temperature 298 K, and stirring speed 200 rpm. To maintain the pH of the medium, either 0.1 M NaOH or HCl was added to set a particular pH value.
- Influence of contact period was conducted through the periods (0, 5, 10, 15, 20, 30, 45, 60, 75, 90, 105, 120, 150, 180, 360, 420, and 480 min), LLP@Fe_3O_4 dosage 50 mg, solution volume 30.0 mL, concentration 20.8 mg/g, pH 5.1, temperature 298 K, and agitation speed 200 rpm.
- The influence of stirring speed was examined under seven varying speeds (0, 50.0, 100.0, 150.0, 200.0, 250.0, and 300.0 rpm), pH 5.1, contact period 120 min, concentration 20.8 mg/L, solution volume 30.0 mL, temperature 298 K, and LLP@Fe_3O_4 dosage 50 mg.
- LLP@Fe_3O_4 dosage was examined using different weights (10, 20, 30, 40, 50, 60, 70, and 80 mg/30 mL) of adsorbent, pH 5.1, contact time 120 min, concentration 20.8 mg/L, solution volume 30.0 mL, stirring speed 200 rpm, and temperature 298 K.
- The influence of initial MO concentration was conducted using 20.8, 40.4, 59.7, 79.2, 98.7, 142.1, and 201.7 mg/L, pH 5.1, time 120 min, LLP@Fe_3O_4 dosage 50 mg, stirring speed 200 rpm, and temperature 298 K.
- The influence of temperature was examined under varied temperatures of 298, 308, 318, and 328 K, pH 5.1, time 120 min, LLP@Fe_3O_4 dose 50.0 mg, solution volume 30.0 mL, and stirring speed 200 rpm.

In all experiments, the vials were shaken using an incubator shaker. After reaching equilibrium, the adsorbents were separated by means of an external magnet, and the MO concentration in the filtrate was estimated using a UV–Visible spectrophotometer. Each experiment was carried out in duplicate and the average of two values was used for the calculation of design parameters.

The quantity of dye adsorbed was calculated by the variance between the beginning and equilibrium concentrations. The removal efficiency (%) was estimated by Eq. (1):

$$\%\ MO\ \text{Removal} = \left(\frac{C_o - C_e}{C_o}\right) \times 100 \tag{1}$$

The sorption efficiency [the quantity of dye adsorbed per gram sorbent (mg/g)] was computed using Eq. (2):

$$q_e = \frac{(C_o - C_e)\ V}{M} \tag{2}$$

2.7. Kinetics, isotherms, and thermodynamic studies

The data was analyzed using IPD, PSO, Elovich, and PFO models to determine the sorption kinetics of MO. The experimental data was acquired by combining 50 mg of LLP@Fe_3O_4 with 30 mL of pH 5.1 effluent solution and changing the contact period (0–480 min). The isotherm tests were carried out by diluting the materials to a set volume (30 mL), LLP@Fe_3O_4 dose (50 mg), pH 5.1, contact period 120 min, and temperature 298 K. D-R, Langmuir, Temkin, and Freundlich isotherms were used to examine the data. Thermodynamic variables such as entropy (ΔS^o), Gibbs free energy (ΔG^o), and enthalpy (ΔH^o) were estimated using data acquired at various temperatures (298–328 K).

2.8. Desorption and reusability of LLP@Fe_3O_4

The H_2SO_4, NaOH, and HCl (1.0 M) eluents were used for the desorption test of MO dye. The adsorption procedure was carried out using the following procedure: 50 mg of LLP@Fe_3O_4 was added to the solution containing 30 mL of 20.8 mg/L of MO dye for 120 min under 200 rpm at 298 K. After adsorption, LLP@Fe_3O_4 was separated using external magnet from the mixture, dried and dye desorption analysis was done, which was combined with 30 mL of an eluting agent, which is stirred for 120 min. The below equation was used to calculate the desorption (%) of MO dye:

$$Desorption\ (\backslash\%)) = \frac{MO_{\ desorbed}}{MO_{\ adsorbed}}\ X\ 100 \tag{3}$$

When MO dye was estimated using all the desorbing agents, NaOH proved to be effective, and this was subsequently investigated for the desorption of MO dye from the conjugates in the concentration range of 0.2 to 1.0 M. To test the conjugate's capacity for regeneration, up to five cycles of adsorption–desorption were carried out using this eluting agent.

2.9. Error functions

In both isotherm and kinetic studies, non-linear regression analysis was performed, and the best models fitting the experimental data were chosen based on the coefficient of determination (R^2) values as well as the error functions, including the SSE, ARE, RMSE, and χ^2, the calculated formulas for which are given below. Greater R^2 and lower SSE, ARE, RMSE, and χ^2 values suggest that the related model is well-fitting.

$$SSE = \sum_{i=1}^{n} (q_{e,\exp} - q_{e,cal})^2 \quad (4)$$

$$ARE = \frac{100}{n} \sum_{i=1}^{n} \left(\frac{q_{e,\exp} - q_{e,cal}}{q_{e,\exp}} \right) \quad (5)$$

$$RMSE = \sqrt{\frac{1}{n-2} \sum_{i=1}^{n} (q_{e,\exp} - q_{e,cal})^2} \quad (6)$$

$$\chi^2 = \sum_{i=1}^{n} \left(\frac{(q_{e,\exp} - q_{e,cal})^2}{q_{e,cal}} \right) \quad (7)$$

3. Results and discussion

3.1. Characterization (FT-IR, FE-SEM with EDX, BET, XRD, SQUID-VSM, and pH_{PZC})

The FT-IR technique is useful for determining the distinctive functional groups that allow for adsorption behavior. The results of FTIR analysis for LLP, LLP@Fe_3O_4, and MO-loaded LLP@Fe_3O_4 are illustrated in Fig. 1. In the LLP spectrum (Fig. 1a), the broadband at 3429 cm^{-1} represented the stretching vibration of –OH and –NH groups due to hydrogen bonds of compounds such as alcohols, carboxylic acids and phenols [38]. The peak at 2929 cm^{-1} corresponded to the C–H vibrations of the stretch methoxy (O-CH_3), methylene (CH_2), and methyl (CH_3) groups, the main components of pectin and lignin [39]. The band at 2363 cm^{-1} represents -C≡C stretching vibrations in alkyne groups [40]. The band at 1654 cm^{-1} was the characteristic of the stretching vibration of C = O from COOH with an intermolecular hydrogen bond [28]. The peak at 1544 cm^{-1} was associated with C = C vibration in the structure of cellulose and lignin. The band observed at 1454 cm could be assigned to symmetric bending vibrations of –CH_3 [41]. The band at 1322 cm^{-1} revealed the existence of antisymmetric stretching of the carboxylate anion [36]. The peak near around 1070 cm^{-1} could be attributed to the stretching vibration of C-O-C and the bending vibration of –OH in the lignin structure of the LLP [39]. The peaks between 800 and 600 show the presence of antisymmetric out-of-plane aromatic ring stretch. After loading Fe_3O_4 nanoparticles, the characteristic peak at 585 cm^{-1} corresponding to Fe-O stretching vibration occurred in LLP@Fe_3O_4 (Fig. 1b), manifesting the success of Fe_3O_4 loading [37]. And the intensities of some bands became shifted (3429, 2929, 2363, 1654, 1454, 1322, and 1070 cm^{-1} to 3425, 2933, 2358, 1633, 1436, 1320, and 1084 cm^{-1}) compared to LLP and one peak even disappeared (1544 cm^{-1}), indicating some functional groups of LLP were linked with Fe_3O_4 nanoparticles. The distinctive alterations seen in the FT-IR spectrum of LLP@Fe_3O_4 after MO adsorption indicated that several bands were displaced or disappeared (Fig. 1c). These variations in the spectrum indicated that dye molecules interacted with the functional groups of the LLP@Fe_3O_4 during the sorption process.

The surface morphologies and elemental compositions of LLP, LLP@Fe_3O_4 before and after adsorption were analyzed using FE-SEM/EDX analysis. The obtained FE-SEM images, EDX, and percentage composition of elements (Wt and At) results are represented in Fig. 2. As displayed in Fig, 2a, it could be seen that the surface of LLP was smooth and irregular. After modifying the LLP with magnetic Fe_3O_4 nanoparticles (Fig. 2b), the LPP@Fe_3O_4 surface was changed into a rough,

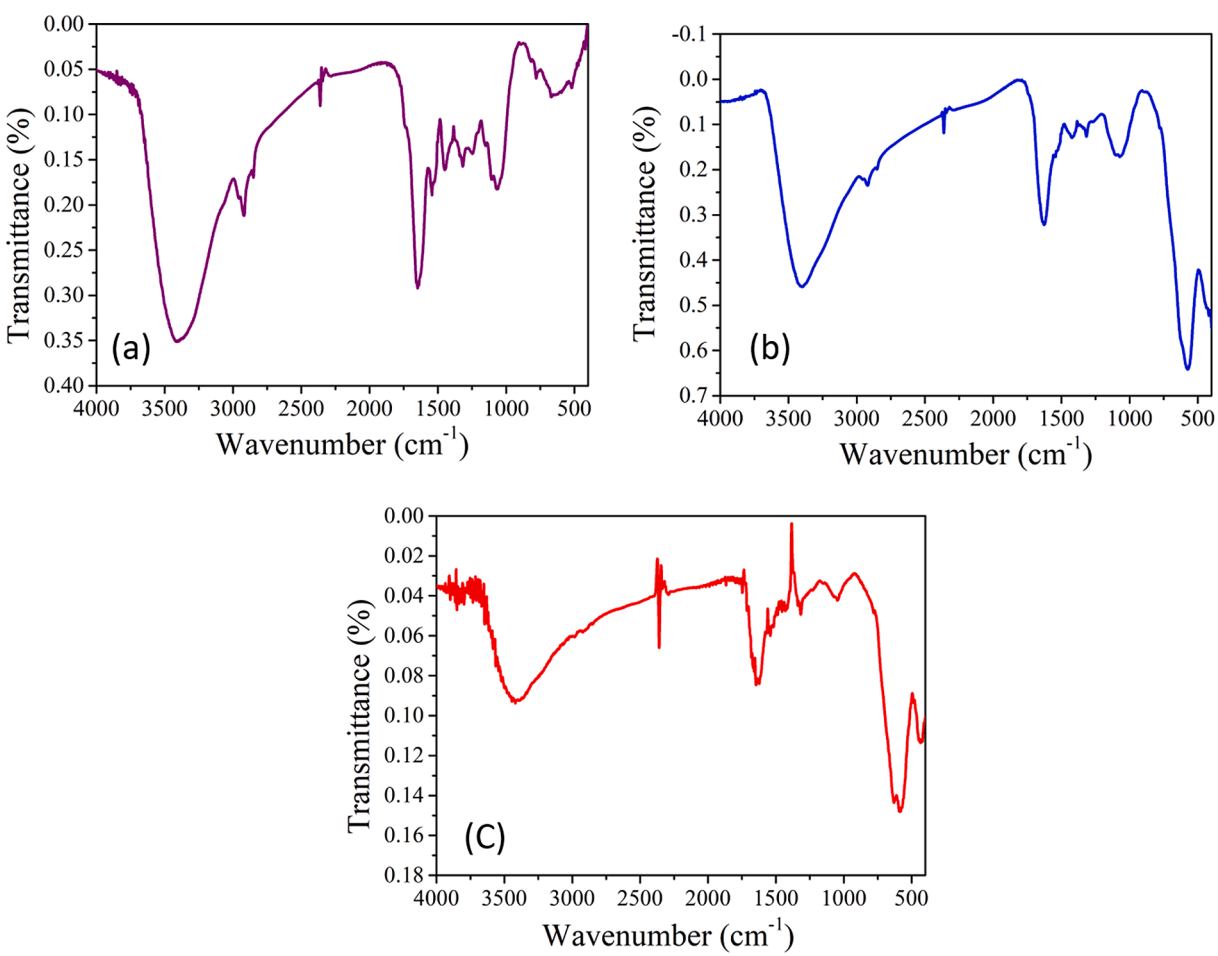

Fig. 1. FT-IR spectrum of (a) LLP, (b) LLP@Fe_3O_4, and (c) MO/LLP@Fe_3O_4.

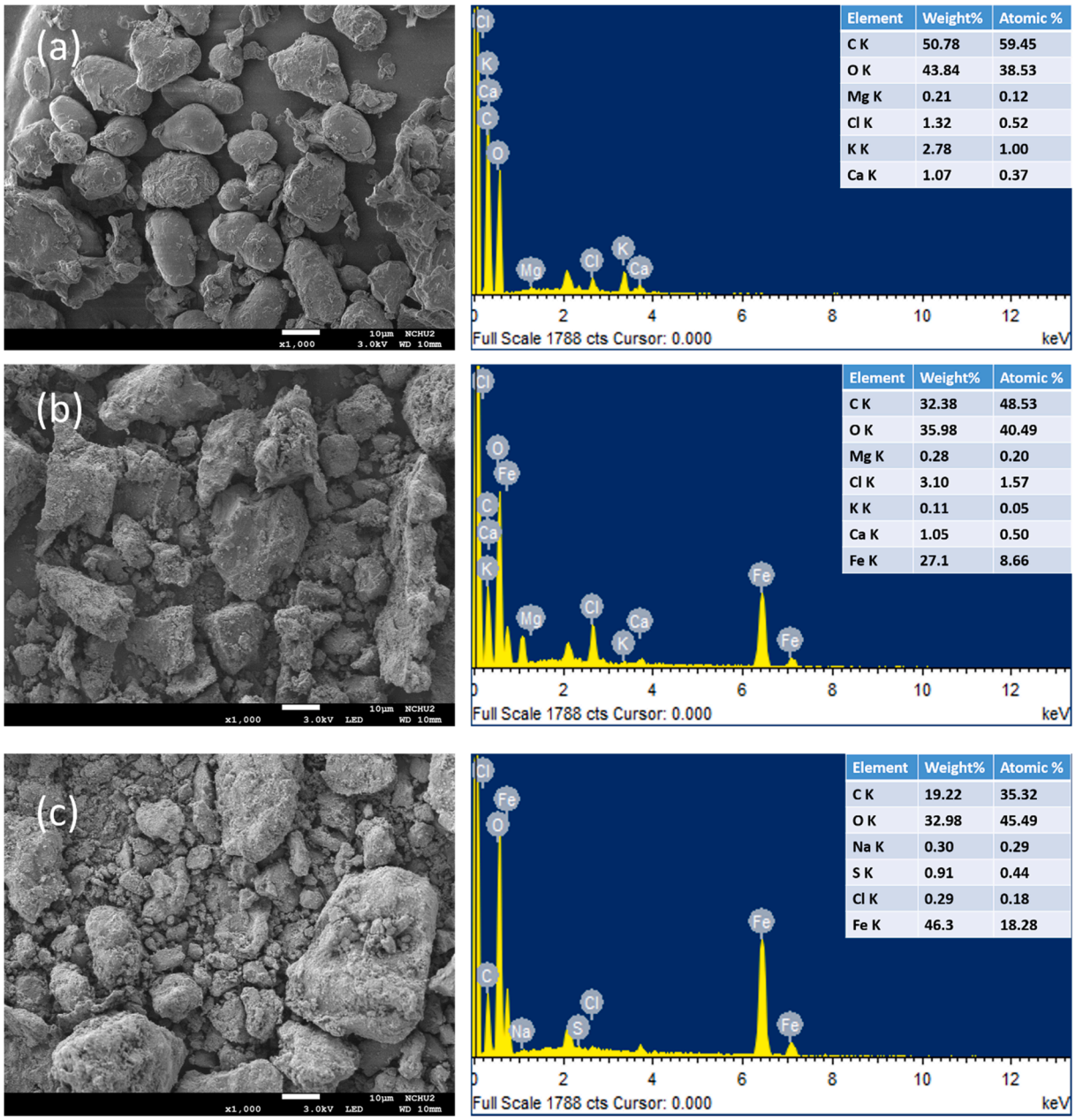

Fig. 2. FE-SEM/EDX images of (a) LLP, (b) LLP@Fe_3O_4, and (c) MO/LLP@Fe_3O_4.

heterogeneous, irregular, and porous surface structure with particles of different sizes and shapes. These changes indicate that the LPP surface was successfully loaded with Fe_3O_4. Adsorbent surface roughness and pores, in general, have an important role in dye adsorption efficacy because they give a large interior surface area [42]. The surface of the LPP@Fe_3O_4 was completely filled by the MO dye molecules after MO adsorption (Fig. 2c), and the surface became smoother, confirming the successful adsorption of MO onto LPP@Fe_3O_4. The EDX analysis shows the presence of C, O, Mg, Cl, K, and Ca elements in the pure LLP before Fe_3O_4 loading and the presence of the Fe element in addition to C, O, Mg, Cl, K, and Ca in the LLP after Fe_3O_4 loading. This indicated the successful incorporation of Fe_3O_4 in the LLP. The EDX spectrum of LLP@ Fe_3O_4 after MO adsorption exhibited the presence of C, O, Na, and S elements [from MO dye molecules] (Fig. 2c), indicating the successful adsorption and distribution of MO dye onto the surface of the LLP@ Fe_3O_4 composite.

Fig. 3 depicts the N_2 adsorption–desorption and pore size distribution for LLP and LLP@ Fe_3O_4 using the BET and BJH methods. Both samples' hysteresis loops reveal that their isotherms were IV type according to IUPAC classification, suggesting that they had a mesoporous structure (Fig. 3a). Furthermore, the LLP@ Fe_3O_4 isotherm had a larger hysteresis loop than the LLP, showing that the introduction of iron oxide nanoparticles on the LLP surface enhanced its pore radius and pore volume [32,43]. This finding is supported by the pore size distribution seen in Fig. 3b. The pore radius, BET surface area, and, pore volume, of LLP@Fe_3O_4, were 2.716 nm, 136.5 m^2/g, and 0.431 cc/g, respectively. These results were much greater than that of raw LLP (6.313 m^2/g, 0.039 cc/g, and 1.491 nm). Therefore, the increased surface area, pore radius, and pore volume could further provide more adsorption sites for dye adsorption.

The XRD analysis was carried out for determining the crystalline or amorphous nature of the as-prepared materials. Fig. 4 shows the XRD patterns of LLP and LLP@Fe_3O_4. LLP (Fig. 4a) exhibited an amorphous nature due to the presence of the high content of organic compounds. It

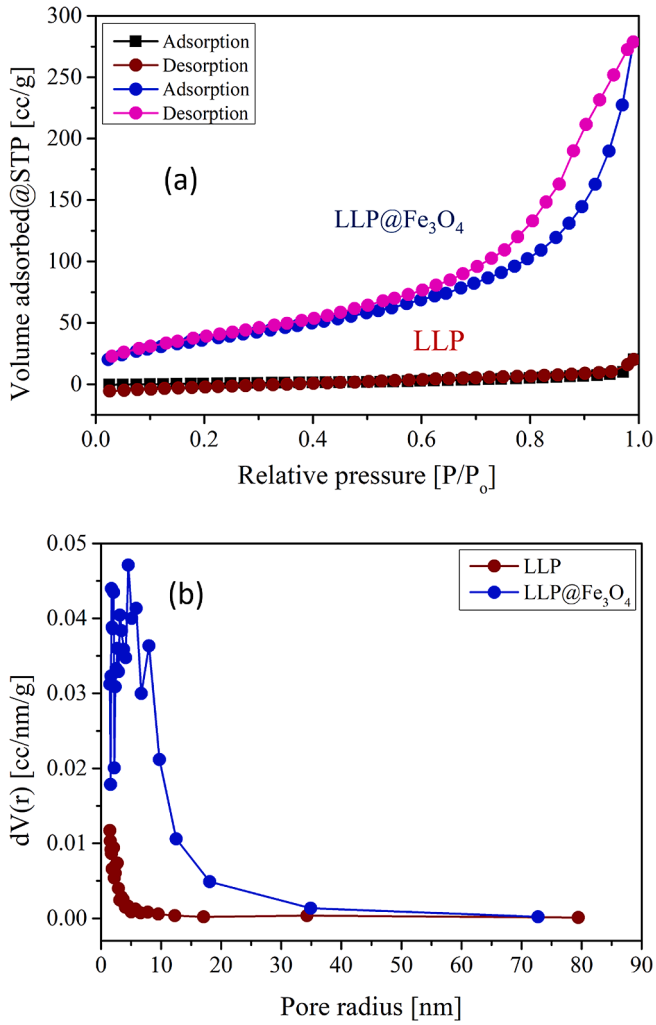

Fig. 3. (a) N_2 adsorption–desorption isotherms and (b) pore size distribution of LLP and LLP@Fe_3O_4.

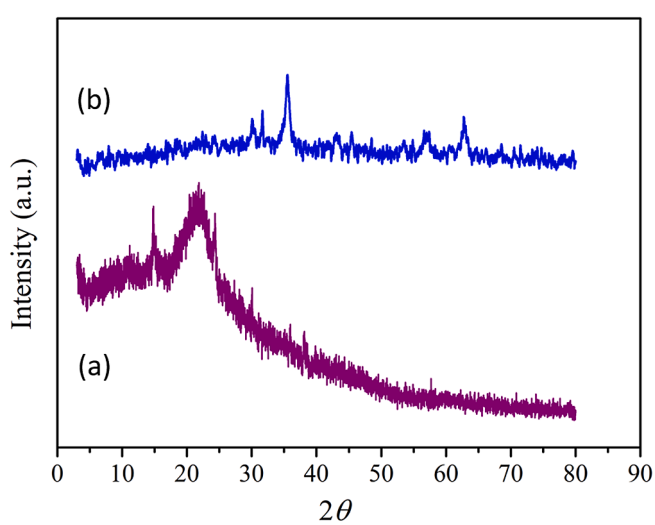

Fig. 4. XRD pattern of (a) LLP and (b) LLP@Fe_3O_4.

displayed broad diffraction peaks at $2\theta = 15.1°$ and 22.3°, which represents the ketones, aldehydes, hydroxyl, and amine groups in the forms of hemicelluloses, lignin, and amorphous cellulose of LLP [44]. The XRD spectra of LLP@Fe_3O_4 can be seen in Fig. 4b. It shows distinct peaks having 2θ values at 30.1°, 35.6°, 43.2°, 53.8°, 57.1°, and 62.8°, which corresponded to the crystal planes of 220.0, 311.0, 400.0, 422.0, 511.0, and 440.0, respectively. The peaks matched the typical magnetite (Fe_3O_4) XRD patterns in JCPDS file No: 19–0629 [45]. These results suggest that the magnetic Fe_3O_4 nanoparticles were loaded on the surface of LLP successfully.

At 298 K, the magnetic characteristics of the LLP@Fe_3O_4 were examined using a SQUID-VSM. Over the applied magnetic field, the magnetization hysteresis loop has a typical S-like shape (as seen in Fig. 5). The zero retentivity and coercivity in the curve revealed the super magnetization of LLP@Fe_3O_4 [46]. The Ms (saturation magnetization) value was determined to be 35.6 emu/g, indicating that the LLP@Fe_3O_4 has superparamagnetic characteristics. Because of these features, the LLP@Fe_3O_4 reacts fast in the presence of an external field and exhibits reversible behaviour in the absence of a magnetic field, making it simple to extract the adsorbent from the reaction liquid after adsorption. As a result, the magnetic characteristics of the adsorbent revealed that the LLP@Fe_3O_4 was a kind of recycled adsorbent that was useful for separation and recovery.

Fig. 6a depicts the LLP@Fe_3O_4 point of zero charge. The obtained pH_{PZC} was 5.5. At this pH level, the charge of the positive surface sites is equal to the charge of the negative surface sites (zero charge on its surface). This variable is crucial because it enables the assessment of the impact of pH on the sorption process by predicting the charge on the biosorbent surface as a function of pH. When in solution, sorbent surfaces are negatively charged when pH is greater than pH_{PZC} and may interact with positive species, whereas solid surfaces are positively charged when pH is lower than pH_{PZC} and may interact with negative species.

3.2. Influence of pH on MO removal and mechanism

The surface charge of a biosorbent and the degree of ionization of the solute is regulated by solution pH, which is important in the sorption process. Fig. 6b depicts the percentage of MO dye adsorption onto LLP@Fe_3O_4 composite from its aqueous solution at various pH levels (1.06–10.2). The removal effectiveness of MO rose from 39.4 to 94.5% as the solution pH climbed from 1.06 to 5.1, and then declined from 83.5 to 10.2% as the pH grew from 6.07 to 10.2. The maximal removal efficiency (94.5%) of MO onto LLP@Fe_3O_4 was obtained at pH 5.1, so, it was identified as the optimal pH for further studies. The uptake of dyes mainly depends upon the pH_{PZC} of the adsorbent and pKa of the dyes [47]. The pH_{PZC} of LLP@Fe_3O_4 was found to be 5.5. At pH less than pH_{PZC}, the surface of the LLP@Fe_3O_4 becomes + vely charged because of the protonation of functional groups (–OH, –NH_2, etc.). While, at pH

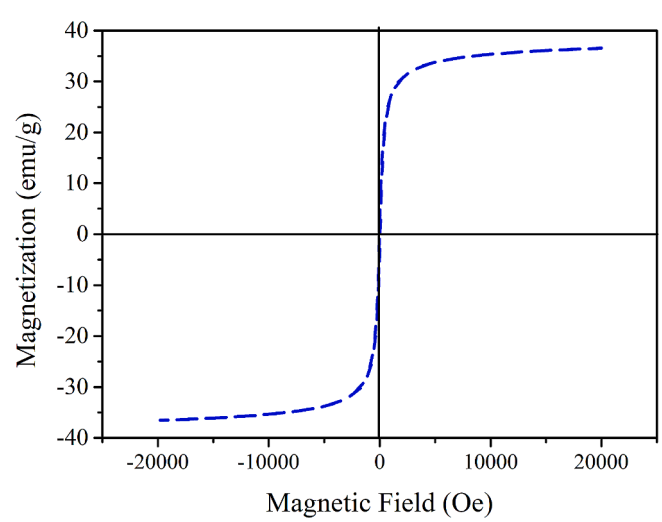

Fig. 5. Magnetization curve of LLP@Fe_3O_4.

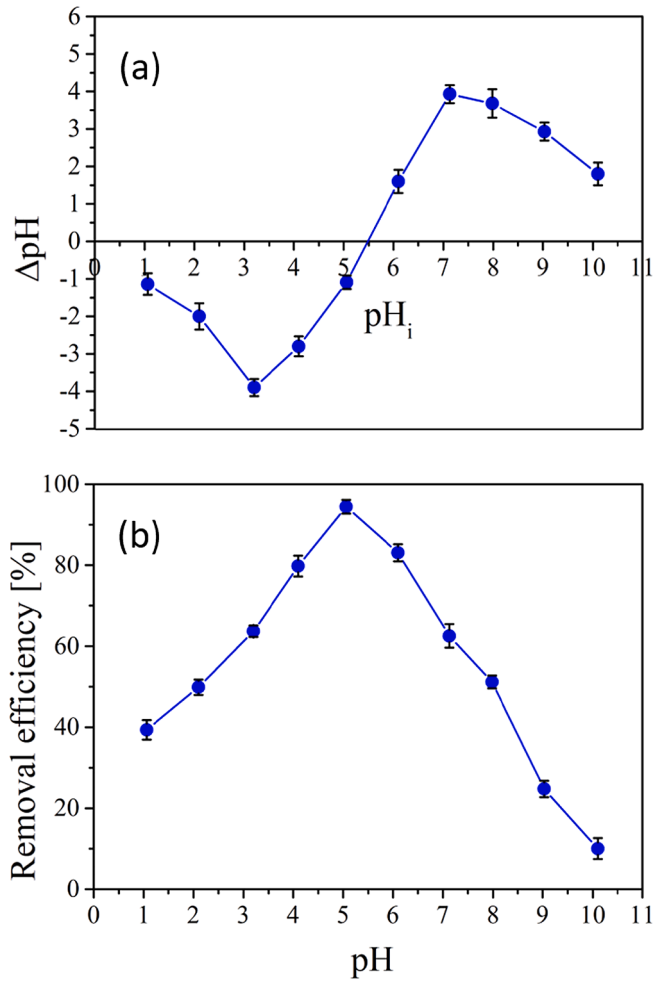

Fig. 6. (a) point of zero charge (pH_{PZC}) of LLP@Fe_3O_4 and (b) effect of pH on the removal of MO onto LLP@Fe_3O_4.

greater than pH_{PZC}, the LLP@Fe_3O_4 surface becomes negatively charged due to the de-protonation. The pKa (dissociation constant) value of MO dye is 3.7 [48]. The MO dye molecule exists in the molecular form at a pH less than pKa [MO-SO_3^- Na^+] while it dissociates at a pH greater than pKa [MO-SO_3^- + Na^+]. The improvement in removal effectiveness with increasing pH from 1.06 to 5.1 may be attributed to electrostatic interaction between + vely charged LLP@Fe_3O_4 surface and -vely charged MO dye molecules. An increase in pH (beyond 5.1) results in a decline in the removal efficiency of MO which may be attributed to the generation of more -vely charged adsorbing sites onto the surface of the LLP@Fe_3O_4 and causes the electrostatic repulsion of negative MO dye molecules. Based on the above discussion, a proposed binding mechanism of MO dye on the LLP@Fe_3O_4 surface is illustrated in Fig. 7. Various studies with MO also found that adsorption was favored at pH below at pH_{PZC} for adsorbents such as modified nitrate intercalated MgAl LDH [49], sugar-based carbon [50], activated carbon/$NiFe_2O_4$ [51], and cationic surfactants modified coffee waste [52].

3.3. Influence of initial concentration on MO removal

One of the major factors describing the partitioning behaviour of the adsorbate molecules between the solid biosorbent and the bulk liquid solution at equilibrium is the initial adsorbate concentration. Using LLP@Fe_3O_4, it was determined how initial MO solution concentrations affected the removal efficiency, and the results are given in Fig. 8a. With an upsurge in MO concentration from 20.8 to 201.1 mg/L, the removal efficiency of MO declined from 94.3 to 44.3% (Fig. 8a). It may be said that having enough active sites on the sorbent surface is what allows for the high removal effectiveness of MO at a low starting dye concentration. Due to competition between the dye and the active binding sites of the sorbent and a lack of available free space to attach dye molecules to the biosorbent surface, the removal effectiveness of MO is reduced at increasing concentrations [53]. It is clearly found that the adsorption of dye depends on the concentration of the pollutants. These findings show that the MO solution concentration of 20.8 mg/L, which was determined to be the proper solution concentration for the adsorption reaction to successfully optimize the process, was where the maximum removal efficiency was seen.

3.4. Effect of LLP@Fe_3O_4 dosage on MO removal

The adsorbent mass is one of the most crucial factors as it reflects the efficiency of the adsorbent for a definite amount of adsorbate during the adsorption process. The impact of LLP@Fe_3O_4 dose on MO dye removal efficiency was investigated by increasing the quantity of LLP@Fe_3O_4 from 10 to 80 mg/30 mL, as displayed in Fig. 8b. The removal efficiency of MO was clearly increased when the LLP@Fe_3O_4 quantity was increased until 50 mg, after which the removal efficiency remained almost comparable. This is due to the availability of a higher number of accessible sorption sites as adsorbent doses increase. However, no significant differences in adsorption performance were identified after 50 mg. Moreover, overuse of adsorbent might cause aggregation of LLP@Fe_3O_4 particles owing to the collision which can limit the accessible adsorption site for incoming dye molecules by decreasing specific surface area and increasing diffusion route length value [54]. At 50 mg doses, the maximal removal effectiveness of MO was up to 94.5%, which may be regarded as an ideal dosage for further experiments.

3.5. Effect of stirring speed on MO removal

In a sorption process, the stirring speed has a considerable impact on both adsorption and adsorbate removal. The impact of stirring speed on the elimination of MO by LLP@Fe_3O_4 has been examined from 0 to 300 rpm. The observed change is displayed in Fig. 8c. MO removal efficiency was 25% without agitation; however, increasing the stirring speed from 50 to 200 rpm boosted removal effectiveness from 42 to 94.3%. This phenomenon may be elucidated by the fact that the diffusion rate of solutes from the bulk liquid to the liquid boundary layer surrounding the biosorbent particles rises quicker as turbulence increases and the thickness of the liquid boundary layer reduces [55]. As the agitation speed further increased (300 rpm), the MO adsorption rate decreased to 87%. The lower removal efficiency might be ascribed to the low adsorption energy between MO dye molecules and the LLP@Fe_3O_4. This occurrence is known as desorption which is not beneficial in terms of sorption performance [56]. The optimum removal effectiveness is achieved at a speed of 200 rpm, which also provides the best uniformity of the mixed suspension. As a result, a speed of 200 rpm was taken for the next tests.

3.6. Effect of contact time on MO removal

The solution/solid reaction time is a crucial factor to analyze the time required for attaining the saturation of the sorption process. The impact of the contact period on the adsorption of MO by LLP@Fe_3O_4 was examined at various time intervals ranging from 0 to 480 min, as depicted in Fig. 8d. It was projected that the removal efficiency of MO would be quick at first, then slow down until equilibrium (saturation) was attained. After reaching equilibrium, no substantial change was noticed. Initially, more binding moieties sites were present on the adsorbent surface for dye ion binding, which is why the dye was removed quickly at the beginning. Alternatively, as the reaction time progresses, the active binding sites are occupied and competition for the remaining dye molecules may arise, slowing dye adsorption at later

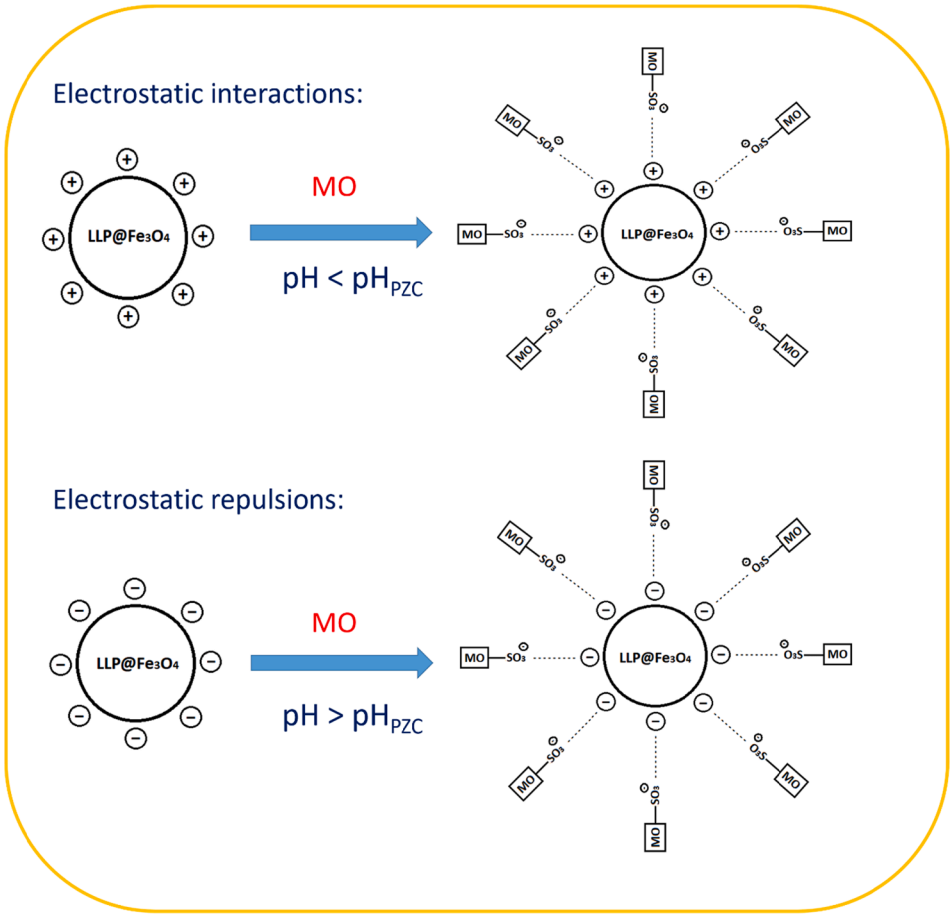

Fig. 7. Proposed adsorption mechanism of MO onto LLP@Fe_3O_4.

stages [57]. The equilibrium was reached in 120 min, confirming that 120 min is necessary to full fill all adsorption-binding sites of LLP@Fe_3O_4 with MO dye molecules. As a result, a contact period of 120 min was chosen for further adsorption investigations. The results of this experiment are used to establish the kinetic parameters of adsorption and make predictions about the nature of the adsorption process.

3.7. Reaction kinetic models

Adsorption reaction kinetics illustrates the biosorption system's sorption behaviour and uptake rate up to equilibrium. The type and sequence of the reaction, which reveal the sorptive profile and effectiveness of the sorbent, are determined using the reaction kinetic model using time study data. The widely used PFO, PSO, and Elovich reaction kinetic models are used in this study, and the model equations are as follows:

$$q_t = q_{e1}(1 - \exp(-k_1 t)) \tag{8}$$

$$q_t = \frac{q_{e2}^2 k_2 t}{1 + q_{e2} k_2 t} \tag{9}$$

$$q_t = \frac{1}{\beta}\ln(1 + \alpha\beta t) \tag{10}$$

The fitting results of the non-linearized PSO, PFO, and Elovich kinetic models are shown in Fig. 9, and the variables along with error function (SSE, ARE, RMSE, and χ^2) values are given in Table 3. The PFO model's correlation coefficient ($R^2 = 0.9681$) reveals some differences in the kinetic predictions of MO adsorption on LLP@Fe_3O_4. The Elovich model is often employed for systems with heterogeneous surfaces; however, the correlation coefficient ($R^2 = 0.9413$) indicates that the Elovich model does not adequately fit the kinetic data, showing that diffusion is not a rate-limiting phenomenon at the interface. The PSO model, on the other hand, has a higher correlation ($R^2 = 0.9989$) and lower SSE (6.33), ARE (2.01), RMSE (3.99), and χ^2 (9.18) values than the PFO and Elovich models. Furthermore, the PSO kinetic model's predicted adsorption capacity was close to the experimental results. As a consequence, the PSO model proved more suitable for modelling the kinetic adsorption process, demonstrating that MO chemisorption on LLP@Fe_3O_4 occurs.

3.7.1. Intra-particle diffusion (IPD)

The IPD model, proposed by Weber-Morris, was used to identify the diffusion mechanism of the process. Its mathematic expression can be given as follows:

$$q_t = K_{id}(t)^{0.5} + C \tag{11}$$

The linear IPD model plot is shown in Fig. 10. Three distinct linear parts were identified, indicating that the MO dye adsorption on the LLP@Fe_3O_4 occurs in three steps. The first, sharper section is ascribed to adsorbate diffusion through the solution to the adsorbent's exterior surface or boundary layer diffusion of solute molecules. The second, linear component is the gradual equilibrium stage, which is dominated by IPD. The third section is ascribed to the final equilibrium stage, during which IPD began to decelerate owing to the very low adsorbate concentration remaining in the solution [58]. The three linear sections of the IPD model did not pass through the origin (C not equal 0), indicating that IPD is not the only rate-limiting phase in the MO dye sorption process on LLP@Fe_3O_4. As a result, both boundary layer diffusion and IPD are engaged in the MO adsorption processes. As shown in Table 3,

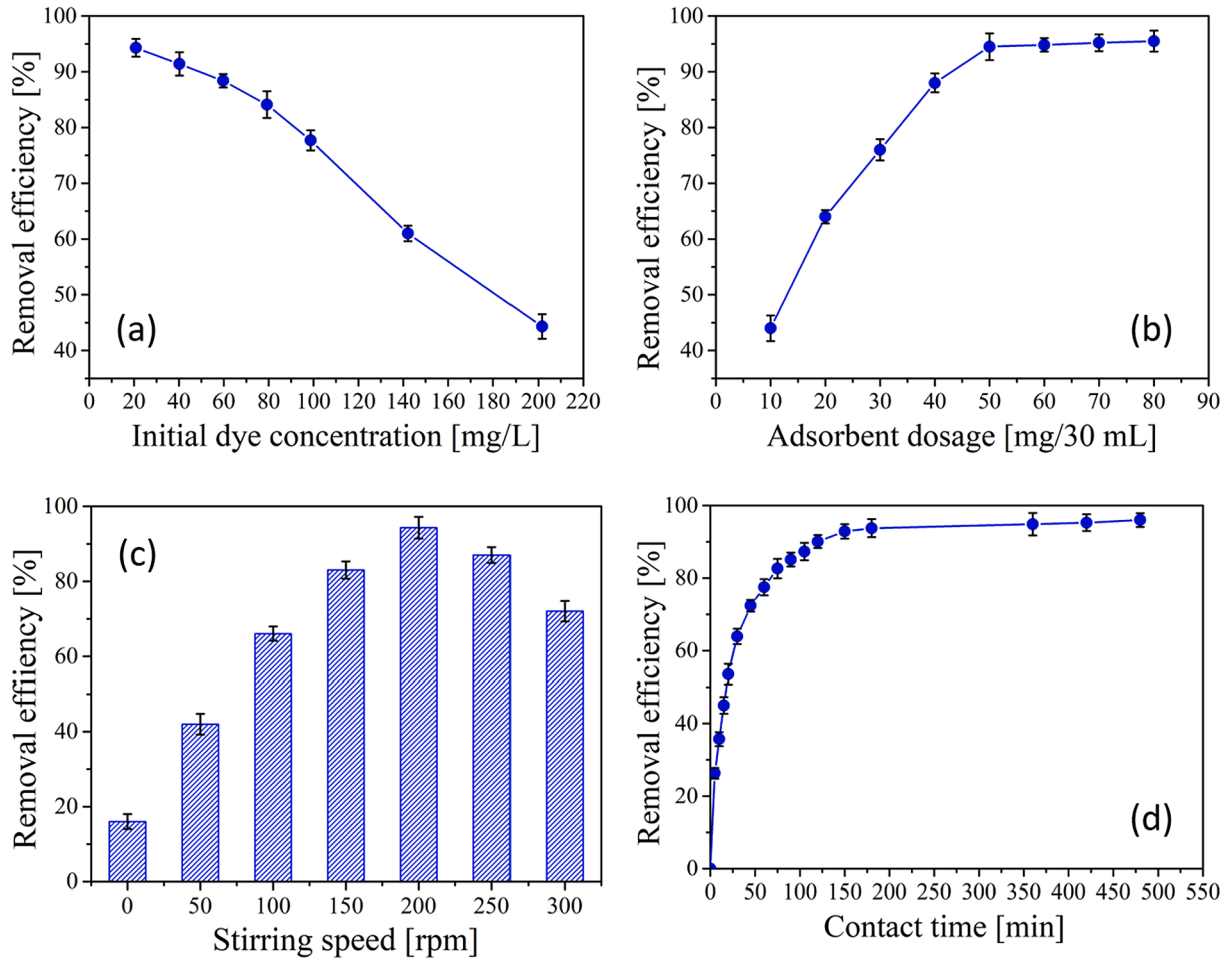

Fig. 8. Effect of (a) initial dye concentration, (b) adsorbent dosage, (c) stirring speed, and (d) contact time on the removal of MO by LLP@Fe_3O_4.

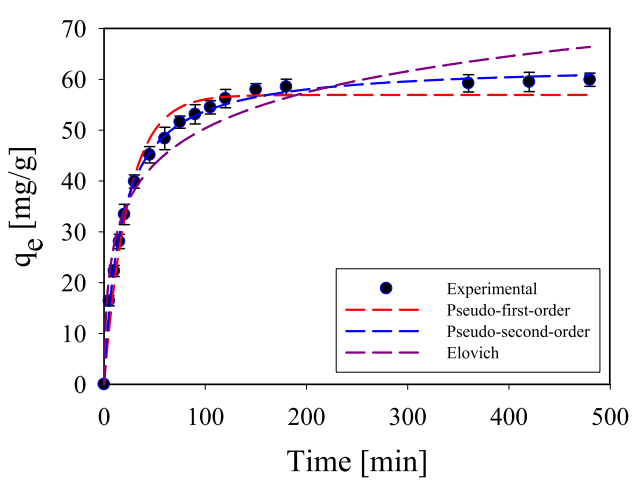

Fig. 9. Non-linear pseudo-first-order, pseudo-second-order, and Elovich kinetics plot for MO dye onto LLP@Fe_3O_4.

the K_{id} values are in the sequence $K_{id,1} > K_{id,2} > K_{id,3}$, showing a strong transfer of dye in solution to the adsorbent's exterior surface and little intraparticle diffusion, presumably due to the quick creation of multilayers, until the adsorbate in solution decreases. C_1, C_2, or C_3 values were not equal to zero, demonstrating the lack of simplex IPD in any of the three phases [59,60].

Table 3
Kinetic parameters for the adsorption of MO onto LLP@Fe_3O_4 at 20.8 mg/L.

Kinetic model	Parameter	Value	Error analysis	Value
Experimental	$q_{e,\ exp}$ (mg/g)	61.83		
Pseudo-first-order	$q_{e1,\ cal}$ (mg/g)	55.91	SSE	25.61
	k_1 (1/min)	0.0418	ARE	8.73
	R^2	0.9681	RMSE	19.36
			χ^2	38.72
Pseudo-second-order	$q_{e2,\ cal}$ (mg/g)	63.02	SSE	6.33
	k_2 (g/mg min)	0.0009	ARE	2.01
	R^2	0.9989	RMSE	3.99
			χ^2	9.18
Elovich	α (mg/g min)	13.81	SSE	34.26
	β (g/mg)	0.0975	ARE	17.42
	R^2	0.9413	RMSE	23.93
			χ^2	67.46
Intra-particle diffusion	$k_{id,1}$ (mg/g $min^{0.5}$)	7.518	SSE	16.61
	C_1 (mg/g)	1.288	ARE	7.68
	R_1^2	0.9888	RMSE	13.42
			χ^2	22.35
	$k_{id,2}$ (mg/g $min^{0.5}$)	2.645	SSE	28.67
	C_2 (mg/g)	27.953	ARE	13.81
	R_2^2	0.9611	RMSE	19.39
			χ^2	47.93
	$k_{id,3}$ (mg/g $min^{0.5}$)	0.177	SSE	58.83
	C_3 (mg/g)	55.931	ARE	31.75
	R_3^2	0.9231	RMSE	43.37
			χ^2	92.36

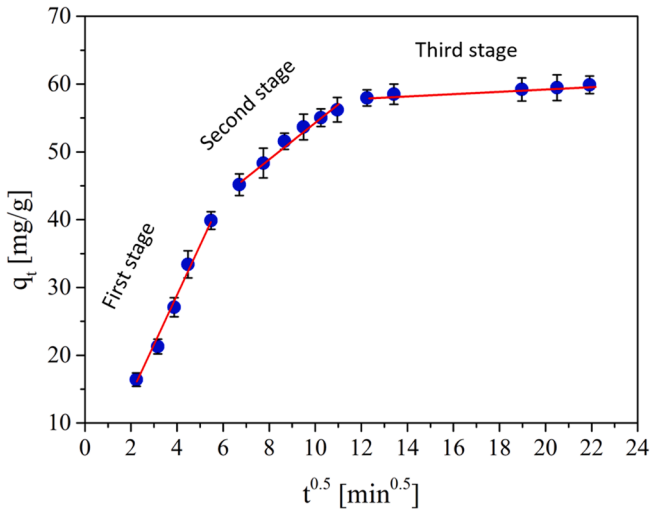

Fig. 10. Weber-Morris (intra-particle diffusion) model for MO adsorption by LLP@Fe_3O_4.

3.8. Adsorption isotherms

When adsorption approaches equilibrium, sorption isotherms characterize the distribution of adsorbate molecules in the liquid medium and the sorbent. The equilibrium results are critical for describing sorption because understanding the adsorption of adsorbed molecules from the liquid medium to the sorbent surface is dependent on the appropriate description of the separation of liquid and solid phases to equilibrium. The adsorption data of MO dye onto LLP@Fe_3O_4 were fitted to D-R, Langmuir, Temkin, and Freundlich models.

The Langmuir isotherm model implies the creation of an adsorbed layer of unimolecular thickness and takes into account the one-to-one interaction between adsorbent and adsorbate. The mathematical equation for this model is represented as:

$$q_e = \frac{q_{\max} K_L C_e}{1 + K_L C_e} \tag{12}$$

The maximal sorption efficiency of LLP@Fe_3O_4 for MO dye was reported to be 282.3 mg/g at 298 K using the Langmuir model. As one of the essential aspects of the Langmuir, a dimensionless constant termed the separation factor (R_L) was computed from the starting concentrations. The R_L is determined by:

$$R_L = \frac{1}{(1 + K_L C_o)} \tag{13}$$

Due to the R_L value, Langmuir's isotherm's kind could be identified with ease. If $R_L = 0$, the isotherm would be kind of irreversible, favourable if $0 < R_L < 1$, unfavourable if $R_L > 1$, and linear if $R_L = 1$. The achieved R_L values at a different initial concentration of MO values were given in Table 4. The achieved R_L values were between 0 and 1.0, indicating the spontaneity and favourability of the adsorption process.

Table 4
Calculated Langmuir separation factor (R_L) for the adsorption of MO onto LLP@Fe_3O_4.

Initial concentration of MO (mg/L)	Separation factor (R_L) derived from the Langmuir model
20	0.2063
40	0.1149
60	0.0797
80	0.061
100	0.0494
140	0.036
200	0.0253

Freundlich's model of adsorption characterizes it as a process of heterogeneous multilayer development caused by the adsorbate molecules' non-uniform affinity and heat of adsorption of active sites on the sorbent surface. It is assumed that once sorption sites on the adsorbent are completed, adsorption energy decreases exponentially. This isotherm applies to the multilayer adsorption of solute molecules onto a heterogeneous surface with a non-uniform heat of sorption distribution. The non-linear equation for this model is given as:

$$q_e = K_f C_e^{1/n} \tag{14}$$

The degree of nonlinearity between the sorbent and the solution concentration depends on the value of n [61]:

- If n is smaller than 1; adsorption process is chemical
- If n exceeds 1; adsorption process is physical
- If n is 1; adsorption is linear

The Freundlich equation n value was discovered to be 4.1. Because n is between 1.0 and 10.0, this indicates that MO is physically adsorbed onto LLP@Fe_3O_4.

The Temkin model has a component that specifically accounts for the interactions between the sorbent and sorbate. Because of the interactions between the adsorbent and adsorbate, the heat of sorption of all the molecules in the layer would drop linearly with coverage. Up to a certain maximum binding energy, the binding energies are distributed uniformly throughout the adsorption process. This model is represented by the following equations:

$$q_e = B_T \ln(A_T C_e) \tag{15}$$

$$q_e = B_T \ln(A_T) + B_T \ln(C_e) \tag{16}$$

$$B_T = \frac{RT}{b_T} \tag{17}$$

The heat of the adsorption process determines the nature of the sorption process, hence the value of B_T, which is the heat constant, determines the type of adsorption. If B_T is positive, it indicates that the sorption process is exothermic, whereas B_T is negative, it suggests that the sorption process is chemically endothermic [62]. In the current study, the B_T value is positive, indicating that the sorption process of MO onto LLP@Fe_3O_4 is exothermic.

The Dubinin-Radushkevich (D-R) is also a widespread isotherm model used for the evaluation of excess adsorption on the surface of LLP@Fe_3O_4. The equations governing this isotherm are given as:

$$q_e = q_m \exp(-\beta \varepsilon^2) \tag{18}$$

$$\varepsilon = RT \ln\left(1 + \frac{1}{C_e}\right) \tag{19}$$

When MO dye molecules are adsorbed on the LLP@Fe_3O_4 sorbent surface from the solution phase, the mean free energy, E, of dye sorption per molecule may be calculated using Eq. (20):

$$E = \frac{1}{\sqrt{2\beta}} \tag{20}$$

Determining the kind of adsorption process is aided by the value of E in the D-R model. Physical interactions are thought to be responsible for the removal of the adsorbate when E is between 1.0 and 8.0 kJ/mol, ion exchange is thought to be involved when E is between 8.0 and 16.0 kJ/mol, and chemical adsorption reactions are indicated by E values>16.0 kJ/mol [63]. In the current study, the value of E is in the range of 1.0 – 8.0 kJ/mol, which indicates that physisorption may contribute to the adsorption of MO onto LLP@Fe_3O_4.

Fig. 11 depicts the non-linear isotherms of the four models. Table 5 also includes the values of various constants and fitting data, including the correlation coefficient R^2, SSE, ARE, RMSE, and χ^2 values. Using the

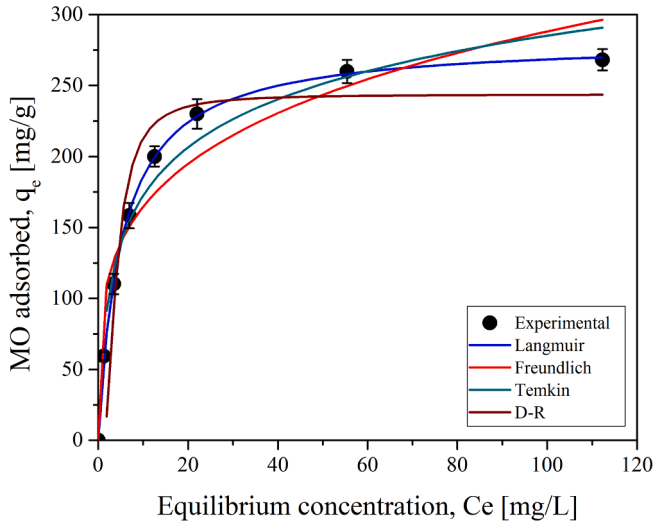

Fig. 11. Non-linear adsorption isotherms plot for MO onto LLP@Fe_3O_4.

Table 5
Isotherm constants for the adsorption of MO onto LLP@Fe_3O_4 at 298 K.

Isotherm model	Parameter	Value	Error analysis	Value
Langmuir	q_m (mg/g)	282.3	SSE	8.81
	K_L (L/mg)	0.1924	ARE	2.27
	R^2	0.9991	RMSE	5.73
			χ^2	10.66
Temkin	B_T (J/mol)	50.66	SSE	141.74
	A_T (L/mg)	3.404	ARE	26.28
	R^2	0.9629	RMSE	79.48
			χ^2	273.12
Freundlich	K_f (mg/g)	94.05	SSE	242.91
	n	4.114	ARE	57.03
	R^2	0.9339	RMSE	127.19
			χ^2	730.65
Dubinin-Radushkevich	q_m (mg/g)	243.77	SSE	673.28
	β (mol^2/J^2)	0.045	ARE	183.63
	E (kJ/mol)	3.33	RMSE	397.71
	R^2	0.8389	χ^2	1187.4

calculated correlation coefficient and error function (SSE, ARE, RMSE, and χ^2) values, the model that best fits the experimental data is determined. The Langmuir R^2 is 0.9991, which is larger than the values for the other three isotherms based on the estimated data from the different models of the two-parameter isotherms. Furthermore, it has the lowest SSE, ARE, RMSE, and χ^2 values. This means that the Langmuir model matches the data better than the other three. This result shows that during the adsorption process, monolayer sorption occurred on a homogeneous surface. The following is the order of the correctness of different isotherms to experimental data: Langmuir > Temkin > Freundlich > D-R.

3.9. Comparison of LLP@Fe_3O_4 with other adsorbents

Table 6 compares the performance of LLP@Fe_3O_4 composite with that of other composites for the adsorption of MO. When compared to other composites described in the literature [48,64–75], the adsorption capability of LLP@Fe_3O_4 displays excellent results, indicating that MO may be readily adsorbed on LLP@Fe_3O_4. The magnetic LLP@Fe_3O_4 composite's greater adsorption capacity might be attributed to its large surface area and functionality. Furthermore, the LLP@Fe_3O_4 may be readily regenerated and isolated from an aqueous solution with little weight loss. According to the comparison, LLP@Fe_3O_4 has a strong adsorption ability for removing MO from an aqueous medium and may be employed as an effective adsorbent.

Table 6
Comparison of maximum adsorption capacity of other adsorbents for MO adsorption.

Adsorbent	Experimental conditions	q_{max} (mg/g)	Reference
Mn@ZnO-NPs	pH = 5.0, T = 303 K	96.154	[48]
Goethite/chitosan beads	pH = 3.0, T = 298 K	84	[64]
Fe_3O_4@MUS composite	pH = 3.0, T = 298 K	149.25	[65]
Fe_3O_4/polypyrrole	pH = -, T = 298 K	149.48	[66]
$MnFe_2O_4$@CPB	pH = 7.0, T = 288 K	90.35	[67]
Magnetic iron oxide/carbon nanocomposites	pH = 4.8, T = 298 K	72.68	[68]
SiO_2-coated Fe_3O_4 nanoparticles	pH = 2.66, T = 298 K	53.19	[69]
PbS/ZnO microspheres	pH = 7.0, T = 298 K	159	[70]
Spent tea leaves/ polyethyleneimine	pH = 3.0, T = 298 K	62.11	[71]
Amine/Fe_3O_4-resin	pH = 5.5, T = 298 K	222.2	[72]
Polyethyleneimine/ β-cyclodextrin/Fe_3O_4	pH = 1.0, T = 303 K	192.2	[73]
MWCNT/SPION	pH = 3.0, T = 298 K	10.54	[74]
Magnetic lignin-based carbon nanoparticles	pH = 5.0, T = 293 K	113	[75]
Magnetic LLP@Fe_3O_4 composite	pH = 5.1, T = 298 K	282.3	Present study

3.10. Temperature effect on MO removal

One of the key factors influencing the actual adsorption action is temperature. It influences both the diffusion of dye molecules within adsorbent pores as well as at the contact of the outer boundary layer of the adsorbent. The sorption process may be exothermic or endothermic depending on the types of dyes and adsorbents [76,77]. The removal effectiveness of LLP@Fe_3O_4 on MO dye in solution at various temperatures (298, 308, 318, and 328 K) was examined in this work. As seen in Fig. 12a, the removal efficiency of MO declined from 94.2 to 74.7% as the temperature increased from 298 to 328 K, showing that the adsorption of MO by LLP@Fe_3O_4 was favorable at low temperatures and exothermic adsorption occurred. This means that at high temperatures, the adsorbent active sites expand and the dye ions and/or molecules in the solution tend to release from the adsorbent surface back into the liquid phases [78]. The maximum removal efficiency of 94.2% was achieved at 298 K, and this temperature was chosen for further studies.

3.11. Thermodynamic analysis

Thermodynamic parameters are crucial for determining the spontaneity of an adsorption process. Gibbs free energy changes (ΔG^o), entropy changes (ΔS^o), and enthalpy changes (ΔH^o) are associated with the adsorption process. These parameters can be calculated from the following Eqs:

$$K_c = \frac{C_{Ae}}{C_e} \tag{21}$$

$$\Delta G^o = \Delta H^o - T\Delta S^o = -RT\ln K_c \tag{22}$$

$$\ln K_c = -\frac{\Delta G^o}{RT} = -\frac{\Delta H^o}{RT} + \frac{\Delta S^o}{R} \tag{23}$$

The ΔG^o was calculated by Eq. (19), and the ΔS^o and ΔH^o can be calculated from the intercept and slope by plotting the $1/T$ versus ln K_c (Fig. 12b). Obtained thermodynamic factors are listed in Table 7. According to the table, the value of ΔG^o is –ve (negative) at all

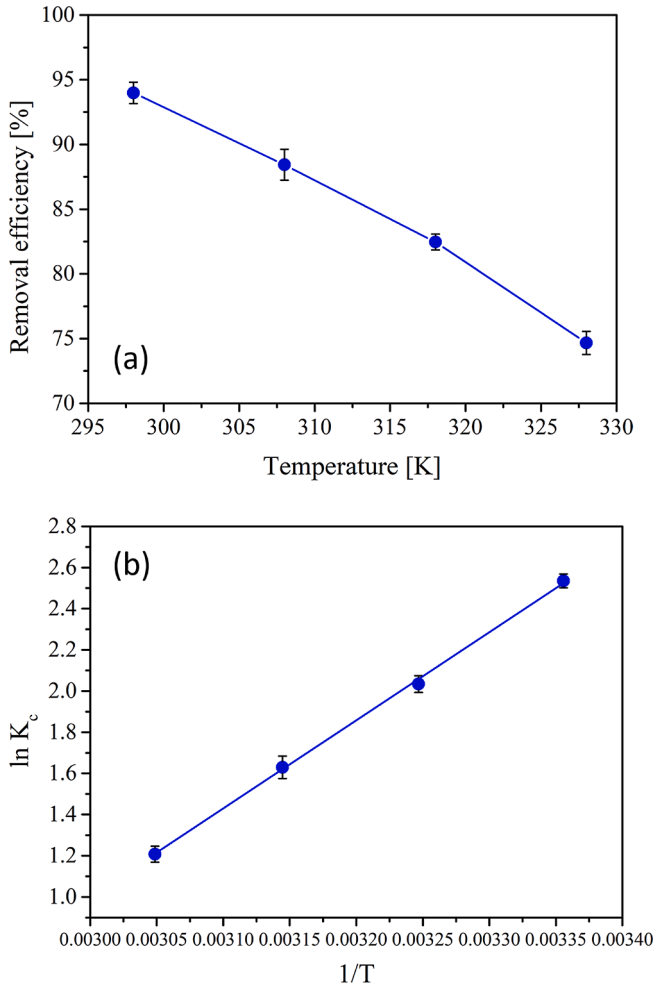

Fig. 12. (a) Effect of temperature on the removal of MO onto LLP@Fe_3O_4 and (b) Van't Hoff plot.

Table 7
Thermodynamic parameters for the adsorption of MO onto LLP@Fe_3O_4 at different temperatures.

Temperature [K]	Thermodynamic parameters			
	ΔG^o (kJ/mol)	ΔS^o (J/mol K)	ΔH^o (kJ/mol)	R^2
298	−6.2808			
308	−5.2083	−98	−35.6	0.9992
318	−4.3081			
328	−3.2949			

temperatures studied, indicating that the adsorption of MO on LLP@Fe_3O_4 is spontaneous [79]. As the temperature rose from 298 to 328 K, the ΔG^o value increased. This implies that when the temperature increases, the spontaneity of the adsorption process reduces. A -ve value for ΔH^o shows that the sorption process is exothermic. As the biosorbent molecule is attracted and subsequently linked to the biosorbent surface, the surface energy of the adsorbate-adsorbent system is lowered due to the newly formed interface, resulting in a -ve adsorption enthalpy [80]. The -ve value of ΔS^o denotes a decrease in the degree of irregularity of the adsorption system on the LLP@Fe_3O_4 surface throughout the adsorption process. This finding reveals the compatibility and affinity between the MO dye molecules in solution and the active site of the LLP@Fe_3O_4, as well as good adsorption reversibility [81].

3.12. Desorption and regeneration studies

The most essential aspect of the adsorption study is regeneration. It is critical to reuse the adsorbent in order to make the adsorption process more cost-effective. For this aim, it is better to desorb the adsorbed MO dye first, followed by five successive adsorption–desorption cycles using the LLP@Fe_3O_4 adsorbent. Desorption tests were performed using eluent i.e., HCl, NaOH, and H_2SO_4 (1.0 M). The desorption efficiencies of MO-adsorbed LLP@Fe_3O_4 by HCl, NaOH, and H_2SO_4 were 19.8, 63.5, and 38.9%, respectively. The anionic nature of the dye may have contributed to the higher desorption of NaOH. Furthermore, to investigate the recycling potential of LLP@Fe_3O_4, desorption was performed using NaOH in the 0.2–1.0 M range, with maximum desorption of 97.1% achieved at 0.2 M NaOH (Fig. 13a). It is worth noting that increasing the NaOH concentration leads to a decrease in desorption efficiency due to the deterioration of active sites present on the LLP@Fe_3O_4 surface [57]. The recovery test was done five times with 0.2 M NaOH, and the results are shown in Fig. 13b. After each cycle, the initially deposited MO dye on the material surface was desorbed by dispersing it in a 0.2 M NaOH solution. The alkalinity of the solution might reduce the strong electrostatic contact between adsorbent and adsorbate, resulting in easier MO dye desorption. The regenerated adsorbent is then dried and reused up to the fifth cycle. According to Fig. 13b, it is clear that the adsorbent's performance decreased after each cycle. The maximal dye removal percentage reached 94.1% in the first cycle and gradually declined to

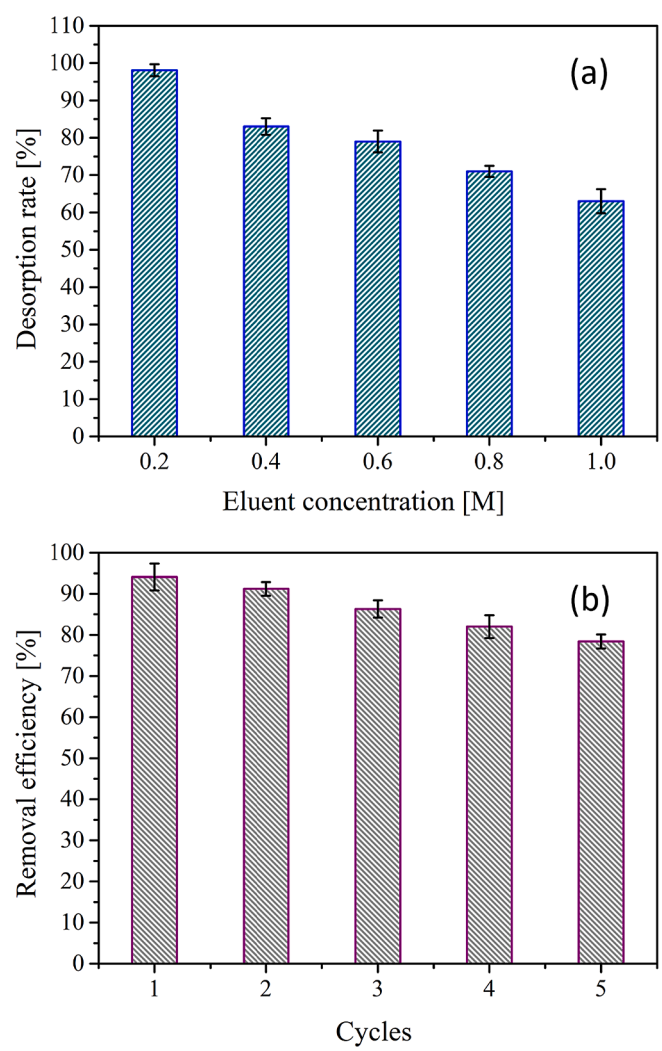

Fig. 13. (a) Desorption and (b) regeneration studies of prepared LLP@Fe_3O_4 for MO dye.

78.4% in the fifth cycle. Between the first and final cycles, the dye removal effectiveness drops to 15.7%. The loss of adsorption sites during the repeated regeneration process may be linked to the decline in adsorption effectiveness [54]. These promising results demonstrated that LLP@Fe_3O_4 has a good regeneration ability and could be repeatedly used for dye removal.

4. Conclusion

In this work, a magnetic separable LLP@Fe_3O_4 nanocomposite was successfully synthesized by the co-precipitation process and applied to adsorbing MO from an aqueous medium. The results of FT-IR, FE-SEM/EDX, XRD, SQUID-VSM, and BJH/BET analysis proved that Fe_3O_4 particles had been successfully loaded on the surface of LLP. The prepared material was a mesoporous structure with a high specific surface area (136.5 m^2/g), which increased the contact possibility between the LLP@Fe_3O_4 and MO. The saturation magnetization (Ms) of LLP@Fe_3O_4 was 35.6 emu/g, which confirms the high separation capability of the nanocomposite by a magnetic field. Experimental data from an evaluation of various influential variables such as LLP@Fe_3O_4 dosage, pH solution, contact period, MO initial concentration, temperature, and agitation speed of the solution were carried out using a batch adsorption method. The highest removal efficiency 94.3 % was obtained at a pH value of 5.1. The adsorption process of MO onto LLP@Fe_3O_4 could be well described by the PSO kinetic model and the Langmuir isotherm model. The maximal adsorption uptake of MO on LLP@Fe_3O_4 was 282.3 mg/g at 298 K. Based on the kinetics and isotherms results, physical and chemical interactions are involved during the adsorption process of MO onto LLP@Fe_3O_4. Thermodynamic studies exhibited an exothermic, feasible, and spontaneous sorption process because of the negative variations in ΔH^o, ΔG^o, and ΔS^o. Even after five consecutive regeneration cycles, the LLP@Fe_3O_4 composite adsorption effectiveness exhibited excellent stability. The electrostatic interactions between the MO and the functional groups on the LLP@Fe_3O_4 surface were responsible for the dye removal. Advantages including eco-friendly, cost-effective, non-toxicity, simple preparation, easy separation, high adsorption efficiency, and high regeneration ability demonstrate that LLP@Fe_3O_4 could be an effective material for the elimination of dyestuff from wastewater.

CRediT authorship contribution statement

Venkata Subbaiah Munagapati: Writing – original draft, Data curation, Methodology, Conceptualization, Visualization, Formal analysis. **Hsin-Yu Wen:** Conceptualization, Validation, Visualization. **Anjani R.K. Gollakota:** Data curation, Formal analysis, Conceptualization. **Jet-Chau Wen:** Conceptualization, Supervision, Resources, Funding acquisition, Data curation, Writing – review & editing. **Chi-Min Shu:** Conceptualization, Writing – review & editing. **Kun-Yi Andrew Lin:** Data curation, Visualization, Writing – review & editing. **Vijaya Yarramuthi:** Data curation, Visualization, Validation. **Jhy-Horng Wen:** Conceptualization. **Guda Mallikarjuna Reddy:** Conceptualization. **Grigory V. Zyryanov:** Conceptualization.

Declaration of Competing Interest

The authors declare that they have no known competing financial interests or personal relationships that could have appeared to influence the work reported in this paper.

Data availability

Data will be made available on request.

Acknowledgements

The authors would like to acknowledge the research support from MOST 110-2625-M-224-001 and 111-2625-M-224-001 by the National Science and Technology Council, Taiwan.

References

[1] J. Men, H. Shi, C. Dong, Y. Yang, Y. Han, R. Wang, Y. Zhang, T. Zhao, J. Li, Preparation of poly(sodium 4-styrene sulfonate) grafted magnetic chitosan microspheres for adsorption of cationic dyes, Int. J. Biol. Macromol. 181 (2021) 810–823, https://doi.org/10.1016/j.ijbiomac.2021.04.079.

[2] H. Behloul, H. Ferkous, N. Bougdah, S. Djellali, M. Alam, C. Djilani, A. Sedik, D. Lerari, B.H. Jeon, Y. Benguerba, New insights on the adsorption of CI-Reactive Red 141 dye using activated carbon prepared from the $ZnCl_2$-treated waste cotton fibers: Statistical physics, DFT, COSMO-RS, and AIM studies, J. Mol. Liq. 364 (2022), 119956, https://doi.org/10.1016/j.molliq.2022.119956.

[3] M.M. Haque, M.A. Haque, M.K. Mosharaf, P.K. Marcus, Decolorization, degradation and detoxification of carcinogenic sulfonated azo dye methyl orange by newly developed biofilm consortia, Saudi, J. Biol. Sci. 28 (2021) 793–804, https://doi.org/10.1016/j.sjbs.2020.11.012.

[4] K. Momina, Ahmad, Remediation of anionic dye from aqueous solution through adsorption on polyaniline/FO nanocomposite-modelling by artificial neural network (ANN), J. Mol. Liq. 360 (2022), 119497, https://doi.org/10.1016/j.molliq.2022.119497.

[5] A.A.A. Darwish, M. Rashad, H.A. AL-Aoh, Methyl orange adsorption comparison on nanoparticles: Isotherm, kinetics, and thermodynamic studies, Dyes Pigm. 160 (2019) 563–571, https://doi.org/10.1016/j.dyepig.2018.08.045.

[6] J. Joseph, R.C. Radhakrishnan, J.K. Johnson, S.P. Joy, J. Thomas, Ion-exchange mediated removal of cationic dye-stuffs from water using ammonium phosphomolybdate, Mater. Chem. Phys. 242 (2020), 122488, https://doi.org/10.1016/j.matchemphys.2019.122488.

[7] N. Uzal, L. Yilmaz, U. Yetis, Nanofiltration and reverse osmosis for reuse of indigo dye rinsing waters, Sep. Sci. Technol. 45 (2010) 331–338, https://doi.org/10.1080/01496390903484818.

[8] N. de C.L. Beluci, G.A.P. Mateus, C.S. Miyashiro, N.C. Homem, R.G. Gomes, M. R. Fagundes-Klen, R. Bergamasco, A.M.S. Vieira, Hybrid treatment of coagulation/flocculation process followed by ultrafiltration in TIO_2 -modified membranes to improve the removal of reactive black 5 dye, Sci. Total Environ. 664 (2019) 222–229, https://doi.org/10.1016/j.scitotenv.2019.01.199.

[9] R. Taheri-Ledari, K. Valadi, S. Gharibi, A. Maleki, Synergistic photocatalytic effect between green LED light and Fe_3O_4/ZnO-modified natural pumice: A novel cleaner product for degradation of methylene blue, Mater. Res. Bull. 130 (2020), 110946, https://doi.org/10.1016/j.materresbull.2020.110946.

[10] V. Soltaninejad, M.R. Ahghari, R. Taheri-Ledari, A. Maleki, Bifunctional PVA/ZnO/AgI/Chlorophyll nanocomposite film: Enhanced photocatalytic activity for degradation of pollutants and antimicrobial property under visible-light irradiation, Langmuir 37 (2021) 4700–4713, https://doi.org/10.1021/acs.langmuir.1c00501.

[11] V. Soltaninejad, A. Maleki, A green, and eco-friendly bionanocomposite film (poly (vinyl alcohol)/TiO_2/chitosan/chlorophyll) by photocatalytic ability, and antibacterial activity under visible-light irradiation, J. Photochem. Photobiol. A: Chem. 404 (2021), 112906, https://doi.org/10.1016/j.jphotochem.2020.112906.

[12] M. Jiang, K. Ye, J. Lin, X. Zhang, W. Ye, S. Zhao, B. Van der Bruggen, Effective dye purification using tight ceramic ultrafiltration membrane, J. Memb. Sci. 566 (2018) 151–160, https://doi.org/10.1016/j.memsci.2018.09.001.

[13] J. Liu, Z. Zhuo, W. Xie, J. Kuo, X. Lu, M. Buyukada, F. Evrendilek, Interaction effects of chlorine and phosphorus on thermochemical behaviors of heavy metals during incineration of sulfur-rich textile dyeing sludge, Chem. Eng. J. 351 (2018) 897–911, https://doi.org/10.1016/j.cej.2018.06.158.

[14] H. Gorzin, A. Ghaemi, A. Hemmati, A. Maleki, Studies on effective interaction parameters in extraction of Pr and Nd using Aliquat 336 from NdFeB magnet-leaching solution: Multiple response optimizations by desirability function, J. Mol. Liq. 324 (2021), 115123, https://doi.org/10.1016/j.molliq.2020.115123.

[15] A. Maleki, Z. Hajizadeh, V. Sharifi, Z. Emdadi, A green, porous and eco-friendly magnetic geopolymer adsorbent for heavy metals removal from aqueous solutions, J. Clean. Prod. 215 (2019) 1233–1245, https://doi.org/10.1016/j.jclepro.2019.01.084.

[16] E.P. Kuncoro, D.R.M. Isnadina, H. Darmokoesoemo, F. Dzembarahmatiny, H. S. Kusuma, Characterization and isotherm data for adsorption of Cd^{2+} from aqueous solution by adsorbent from mixture of bagasse-bentonite, Data Br. 16 (2018) 354–360, https://doi.org/10.1016/j.dib.2017.11.060.

[17] E.P. Kuncoro, D.R.M. Isnadina, H. Darmokoesoemo, O.R. Fauziah, H.S. Kusuma, Characterization, kinetic, and isotherm data for adsorption of Pb^{2+} from aqueous solution by adsorbent from mixture of bagasse-bentonite, Data Br. 16 (2018) 622–629, https://doi.org/10.1016/j.dib.2017.11.098.

[18] E.P. Kuncoro, T. Soedarti, T.W.C. Putranto, H. Darmokoesoemo, N.R. Abadi, H. S. Kusuma, Characterization of a mixture of algae waste-bentonite used as adsorbent for the removal of Pb^{2+} from aqueous solution, Data Br. 16 (2018) 908–913, https://doi.org/10.1016/j.dib.2017.12.030.

[19] R.A. Khera, M. Iqbal, A. Ahmad, S.M. Hassan, A. Nazir, A. Kausar, H.S. Kusuma, J. Niasr, N. Masood, U. Younas, R. Nawaz, M.I. Khan, Kinetics and equilibrium studies of copper, zinc, and nickel ions adsorptive removal on to *Archontophoenix*

alexandrae: conditions optimization by RSM, Desalin. Water Treat. 201 (2020) 289–300, https://doi.org/10.5004/dwt.2020.25937.
[20] Y.A.B. Neolaka, A.A.P. Riwu, U.O. Aigbe, K.E. Ukhurebor, R.B. Onyancha, H. Darmokoesoemo, H.S. Kusuma, Potential of activated carbon from various sources as a low-cost adsorbent to remove heavy metals and synthetic dyes, Results Chem. 5 (2023), 100711, https://doi.org/10.1016/j.rechem.2022.100711.
[21] Y.A.B. Neolaka, Y. Lawa, J. Naat, A.C. Lalang, B.A. Widyaningrum, G.F. Ngasu, K. A. Niga, H. Darmokoesoemo, M. Iqbal, H.S. Kusuma, Adsorption of methyl red from aqueous solution using Bali cow bones (Bos javanicus domesticus) hydrochar powder, Results Eng. 17 (2023), 100824, https://doi.org/10.1016/j.rineng.2022.100824.
[22] Y.A.B. Neolaka, G. Supriyanto, H.S. Kusuma, Adsorption performance of Cr(VI)-imprinted poly(4-VP-co-MMA) supported on activated Indonesia (Ende-Flores) natural zeolite structure for Cr(VI) removal from aqueous solution, J. Environ. Chem. Eng. 6 (2018) 3436–3443, https://doi.org/10.1016/j.jece.2018.04.053.
[23] Y.A.B. Neolaka, Y. Lawa, J.N. Naat, A.A.P. Riwu, H. Darmokoesoemo, G. Supriyanto, C.I. Holdsworth, A.N. Amenaghawon, H.S. Kusuma, A Cr(VI)-imprinted-poly(4-VP-co-EGDMA) sorbent prepared using precipitation polymerization and its application for selective adsorptive removal and solid phase extraction of Cr(VI) ions from electroplating industrial wastewater, React. Funct. Polym. 147 (2020), 104451, https://doi.org/10.1016/j.reactfunctpolym.2019.104451.
[24] Y.A.B. Neolaka, Y. Lawa, J. Naat, A.A.P. Riwu, Y.E. Lindu, H. Darmokoesoemo, B. A. Widyaningrum, M. Iqbal, H.S. Kusuma, Evaluation of magnetic material IIP@GO-Fe_3O_4 based on Kesambi wood (Schleichera oleosa) as a potential adsorbent for the removal of Cr(VI) from aqueous solutions, React. Funct. Polym. 166 (2021), 105000, https://doi.org/10.1016/j.reactfunctpolym.2021.105000.
[25] G. Sriram, A. Bendre, T. Altalhi, H.Y. Jung, G. Hegde, M. Kurkuri, Surface engineering of silica based materials with Ni–Fe layered double hydroxide for the efficient removal of methyl orange: Isotherms, kinetics, mechanism and high selectivity studies, Chemosphere 287 (2022), 131976, https://doi.org/10.1016/j.chemosphere.2021.131976.
[26] A. Zenebe, A.M. Kabir-ud-Din, S. Yimer, H.D. Kuzhunellil, Green synthesis of magnetic nanocomposite by Cordia Africana (CA) leave extract for the treatment of Methylene blue contaminated water, Chem. Eng. J. Adv. 8 (2021), 100193, https://doi.org/10.1016/j.ceja.2021.100193.
[27] A.A. Alqadami, M. Naushad, Z.A. Alothman, T. Ahamad, Adsorptive performance of MOF nanocomposite for methylene blue and malachite green dyes: Kinetics, isotherm and mechanism, J. Environ. Manage. 223 (2018) 29–36, https://doi.org/10.1016/j.jenvman.2018.05.090.
[28] X. Han, W. Wang, X. Ma, Adsorption characteristics of methylene blue onto low cost biomass material lotus leaf, Chem. Eng. J. 171 (2011) 1–8, https://doi.org/10.1016/j.cej.2011.02.067.
[29] B. Tanhaei, A. Ayati, E. Iakovleva, M. Sillanpää, Efficient carbon interlayed magnetic chitosan adsorbent for anionic dye removal: Synthesis, characterization and adsorption study, Int. J. Biol. Macromol. 164 (2020) 3621–3631, https://doi.org/10.1016/j.ijbiomac.2020.08.207.
[30] M. Touihri, F. Guesmi, C. Hannachi, B. Hamrouni, L. Sellaoui, M. Badawi, J. Poch, N. Fiol, Single and simultaneous adsorption of Cr(VI) and Cu(II) on a novel Fe_3O_4/pine cones gel beads nanocomposite: Experiments, characterization and isotherms modeling, Chem. Eng. J. 416 (2021), https://doi.org/10.1016/j.cej.2021.129101.
[31] S. Pai, M.S. Kini, R. Mythili, R. Selvaraj, Adsorptive removal of AB113 dye using green synthesized hydroxyapatite/magnetite nanocomposite, Environ. Res. 210 (2022), 112951, https://doi.org/10.1016/j.envres.2022.112951.
[32] V. Subbaiah Munagapati, H.Y. Wen, A.R.K. Gollakota, J.C. Wen, C.M. Shu, K. Y. Andrew Lin, Z. Tian, J.H. Wen, G. Mallikarjuna Reddy, G.V. Zyryanov, Magnetic Fe3O4 nanoparticles loaded papaya (Carica papaya L.) seed powder as an effective and recyclable adsorbent material for the separation of anionic azo dye, J. Mol. Liq. 345 (2022), 118255, https://doi.org/10.1016/j.molliq.2021.118255. Congo Red) from liquid phase: Evaluation of adsorption properties.
[33] K.G. Akpomie, J. Conradie, Biosorption and regeneration potentials of magnetite nanoparticle loaded Solanum tuberosum peel for celestine blue dye, Int. J. Phytoremediat. 23 (2021) 347–361, https://doi.org/10.1080/15226514.2020.1814198.
[34] C. Prasad, S. Karlapudi, P. Venkateswarlu, I. Bahadur, S. Kumar, Green arbitrated synthesis of Fe_3O_4 magnetic nanoparticles with nanorod structure from pomegranate leaves and Congo red dye degradation studies for water treatment, J. Mol. Liq. 240 (2017) 322–328, https://doi.org/10.1016/j.molliq.2017.05.100.
[35] K.G. Akpomie, J. Conradie, Efficient synthesis of magnetic nanoparticle-Musa acuminata peel composite for the adsorption of anionic dye, Arab. J. Chem. 13 (2020) 7115–7131, https://doi.org/10.1016/j.arabjc.2020.07.017.
[36] J. Geng, J. Chang, Synthesis of magnetic Forsythia suspensa leaf powders for removal of metal ions and dyes from wastewater, J. Environ. Chem. Eng. 8 (2020), 104224, https://doi.org/10.1016/j.jece.2020.104224.
[37] A. Sharma, D. Mangla, A. Choudhry, M. Sajid, S. Ali Chaudhry, Facile synthesis, physico-chemical studies of Ocimum sanctum magnetic nanocomposite and its adsorptive application against Methylene blue, J. Mol. Liq. 362 (2022), 119752, https://doi.org/10.1016/j.molliq.2022.119752.
[38] O.O. Rukayat, M.F. Usman, O.M. Elizabeth, O.O. Abosede, I.U. Faith, Kinetic Adsorption of Heavy Metal (Copper) On Rubber (Hevea Brasiliensis) Leaf Powder, South African, J Chem. Eng. 37 (2021) 74–80, https://doi.org/10.1016/j.sajce.2021.04.004.
[39] M. Peydayesh, A. Rahbar-Kelishami, Adsorption of methylene blue onto Platanus orientalis leaf powder: Kinetic, equilibrium and thermodynamic studies, J. Ind. Eng. Chem. 21 (2015) 1014–1019, https://doi.org/10.1016/j.jiec.2014.05.010.
[40] W.A. Shaikh, A. Kumar, S. Chakraborty, M. Naushad, R.U. Islam, T. Bhattacharya, S. Datta, Removal of toxic dye from dye-laden wastewater using a new nanocomposite material: Isotherm, kinetics and adsorption mechanism, Chemosphere 308 (2022), 136413, https://doi.org/10.1016/j.chemosphere.2022.136413.
[41] M. Tamez Uddin, M. Rukanuzzaman, M. Maksudur Rahman Khan, M. Akhtarul Islam, Adsorption of methylene blue from aqueous solution by jackfruit (Artocarpus heteropyllus) leaf powder: A fixed-bed column study, J. Environ. Manage. 90 (2009) 3443–3450, https://doi.org/10.1016/j.jenvman.2009.05.030.
[42] V. Subbaiah Munagapati, H.Y. Wen, A.R.K. Gollakota, J.C. Wen, K.Y. Andrew Lin, C.M. Shu, G. Mallikarjuna Reddy, G.V. Zyryanov, J.H. Wen, Z. Tian, Removal of sulfonated azo Reactive Red 195 textile dye from liquid phase using surface-modified lychee (Litchi chinensis) peels with quaternary ammonium groups: Adsorption performance, regeneration, and mechanism, J. Mol. Liq. 368 (2022), 120657, https://doi.org/10.1016/j.molliq.2022.120657.
[43] C.E. Almeida-Naranjo, M.B. Aldás, G. Cabrera, V.H. Guerrero, Caffeine removal from synthetic wastewater using magnetic fruit peel composites: Material characterization, isotherm and kinetic studies, Environ. Challenges 5 (2021), 100343, https://doi.org/10.1016/j.envc.2021.100343.
[44] A.K. Prajapati, S. Das, M.K. Mondal, Exhaustive studies on toxic Cr(VI) removal mechanism from aqueous solution using activated carbon of Aloe vera waste leaves, J. Mol. Liq. 307 (2020), 112956, https://doi.org/10.1016/j.molliq.2020.112956.
[45] Z. Hajizadeh, K. Valadi, R. Taheri-Ledari, A. Maleki, Convenient Cr(VI) removal from aqueous samples: Executed by a promising clay-based catalytic system, magnetized by Fe_3O_4 nanoparticles and functionalized with humic acid, ChemistrySelect 5 (2020) 2441–2448, https://doi.org/10.1002/slct.201904672.
[46] S. Zhao, Y. Zhan, X. Wan, S. He, X. Yang, J. Hu, G. Zhang, Selective and efficient adsorption of anionic dyes by core/shell magnetic MWCNTs nano-hybrid constructed through facial polydopamine tailored graft polymerization: Insight of adsorption mechanism, kinetic, isotherm and thermodynamic study, J. Mol. Liq. 319 (2020), 114289, https://doi.org/10.1016/j.molliq.2020.114289.
[47] E.A. Khan, T.A. Shahjahan, Khan, Adsorption of methyl red on activated carbon derived from custard apple (Annona squamosa) fruit shell: Equilibrium isotherm and kinetic studies, J. Mol. Liq. 249 (2018) 1195–1211, https://doi.org/10.1016/j.molliq.2017.11.125.
[48] A. Raza, M. Shoeb, F. Mashkoor, S. Rahaman, M. Mobin, C. Jeong, M. Yusuf Ansari, A. Ahmad, Phoenix dactylifera mediated green synthesis of Mn doped ZnO nanoparticles and its adsorption performance for methyl orange dye removal: A comparative study, Mater. Chem. Phys. 286 (2022), 126173, https://doi.org/10.1016/j.matchemphys.2022.126173.
[49] B.S. Yadav, S. Dasgupta, Effect of time, pH, and temperature on kinetics for adsorption of methyl orange dye into the modified nitrate intercalated MgAl LDH adsorbent, Inorg. Chem. Commun. 137 (2022), 109203, https://doi.org/10.1016/j.inoche.2022.109203.
[50] X. Liu, Y. Wu, H. Ye, J. Chen, W. Xiao, W. Zhou, Z.N. Garba, I. Lawan, L. Wang, Z. Yuan, Modification of sugar-based carbon using lanthanum and cobalt bimetal species for effective adsorption of methyl orange, Environ. Technol. Innov. 23 (2021), 101769, https://doi.org/10.1016/j.eti.2021.101769.
[51] T. Jiang, Y.D. Liang, Y.J. He, Q. Wang, Activated carbon/NiFe2O4 magnetic composite: A magnetic adsorbent for the adsorption of methyl orange, J. Environ. Chem. Eng. 3 (2015) 1740–1751, https://doi.org/10.1016/j.jece.2015.06.020.
[52] R. Lafi, A. Hafiane, Removal of methyl orange (MO) from aqueous solution using cationic surfactants modified coffee waste (MCWs), J. Taiwan Inst. Chem. Eng. 58 (2016) 424–433, https://doi.org/10.1016/j.jtice.2015.06.035.
[53] B.T. Gemici, H.U. Ozel, H.B. Ozel, Removal of methylene blue onto forest wastes: Adsorption isotherms, kinetics and thermodynamic analysis, Environ. Technol. Innov. 22 (2021), 101501, https://doi.org/10.1016/j.eti.2021.101501.
[54] D. Brahma, H. Saikia, Synthesis of ZrO2/MgAl-LDH composites and evaluation of its isotherm, kinetics and thermodynamic properties in the adsorption of congo red dye, Chem. Thermodyn. Therm. Anal. 7 (2022), 100067, https://doi.org/10.1016/j.ctta.2022.100067.
[55] N. Sedira, S. Bouranene, A. Gheid, Ultrasound-assisted adsorption of Pb ions by carbonized/activated date stones from singles/mixed aqueous solutions, J. Indian Chem. Soc. 99 (2022), 100318, https://doi.org/10.1016/j.jics.2021.100318.
[56] A. Kumar Biswal, M. Sahoo, P. Kumar Suna, L. Panda, C. Lenka, P. Kumari Misra, Exploring the adsorption efficiency of a novel cellulosic material for removal of food dye from water, J. Mol. Liq. 350 (2022), 118577, https://doi.org/10.1016/j.molliq.2022.118577.
[57] M. Maqbool, S. Sadaf, H.N. Bhatti, S. Rehmat, A. Kausar, S.A. Alissa, M. Iqbal, Sodium alginate and polypyrrole composites with algal dead biomass for the adsorption of Congo red dye: Kinetics, thermodynamics and desorption studies, Surf. Interfaces 25 (2021), 101183, https://doi.org/10.1016/j.surfin.2021.101183.
[58] S. Chen, C. Qin, T. Wang, F. Chen, X. Li, H. Hou, M. Zhou, Study on the adsorption of dyestuffs with different properties by sludge-rice husk biochar: Adsorption capacity, isotherm, kinetic, thermodynamics and mechanism, J. Mol. Liq. 285 (2019) 62–74, https://doi.org/10.1016/j.molliq.2019.04.035.
[59] H. Shi, C. Dong, Y. Yang, Y. Han, F. Wang, C. Wang, J. Men, Preparation of sulfonate chitosan microspheres and study on its adsorption properties for methylene blue, Int. J. Biol. Macromol. 163 (2020) 2334–2345, https://doi.org/10.1016/j.ijbiomac.2020.09.078.
[60] A.M.A.D. Assis, K.S. da Silva, M.K.S. Araújo, D.C.S. Sales, M.C. Ferreira, A.C.V. de Araújo, W.M. de Azevedo, E.H.L. Falcão, Thermal synthesis of rGO and rGO-Co3O4 and their application as adsorbents for anionic dye removal, Colloids Surfaces A

Physicochem. Eng. Asp. 599 (2020), 124837, https://doi.org/10.1016/j.colsurfa.2020.124837.

[61] H. Boulika, M. El Hajam, M. Hajji Nabih, I. Riffi Karim, N. Idrissi Kandri, A. Zerouale, Definitive screening design applied to cationic & anionic adsorption dyes on Almond shells activated carbon: Isotherm, kinetic and thermodynamic studies, Mater. Today Proc. (2022), https://doi.org/10.1016/j.matpr.2022.07.358.

[62] L. Zafar, A. Khan, U. Kamran, S.J. Park, H.N. Bhatti, Eucalyptus (camaldulensis) bark-based composites for efficient Basic Blue 41 dye biosorption from aqueous stream: Kinetics, isothermal, and thermodynamic studies, Surf. Interfaces 31 (2022), 101897, https://doi.org/10.1016/j.surfin.2022.101897.

[63] X. Yang, W. Zhu, Y. Song, H. Zhuang, H. Tang, Removal of cationic dye BR46 by biochar prepared from Chrysanthemum morifolium Ramat straw: A study on adsorption equilibrium, kinetics and isotherm, J. Mol. Liq. 340 (2021), 116617, https://doi.org/10.1016/j.molliq.2021.116617.

[64] V.S. Munagapati, V. Yarramuthi, D.S. Kim, Methyl orange removal from aqueous solution using goethite, chitosan beads and goethite impregnated with chitosan beads, J. Mol. Liq. 240 (2017) 329–339, https://doi.org/10.1016/j.molliq.2017.05.099.

[65] M.A. Barakat, R. Kumar, E.C. Lima, M.K. Seliem, Facile synthesis of muscovite–supported Fe_3O_4 nanoparticles as an adsorbent and heterogeneous catalyst for effective removal of methyl orange: Characterisation, modelling, and mechanism, J. Taiwan Inst. Chem. Eng. 119 (2021) 146–157, https://doi.org/10.1016/j.jtice.2021.01.025.

[66] M. Zhang, Z. Yu, H. Yu, Adsorption of Eosin Y, methyl orange and brilliant green from aqueous solution using ferroferric oxide/polypyrrole magnetic composite, Polym. Bull. 77 (2020) 1049–1066, https://doi.org/10.1007/s00289-019-02792-1.

[67] Z. Wang, Y. Li, X. Xie, Z. Wang, Bifunctional MnFe2O4/chitosan modified biochar composite for enhanced methyl orange removal based on adsorption and photo-Fenton process, Colloids Surfaces A Physicochem. Eng. Asp. 613 (2021), 126104, https://doi.org/10.1016/j.colsurfa.2020.126104.

[68] R. Istratie, M. Stoia, C. Păcurariu, C. Locovei, Single and simultaneous adsorption of methyl orange and phenol onto magnetic iron oxide/carbon nanocomposites, Arab. J. Chem. 12 (2019) 3704–3722, https://doi.org/10.1016/j.arabjc.2015.12.012.

[69] M. Shariati-Rad, M. Irandoust, S. Amri, M. Feyzi, F. Ja'fari, Magnetic solid phase adsorption, preconcentration and determination of methyl orange in water samples using silica coated magnetic nanoparticles and central composite design, Int. Nano Lett. 4 (2014) 91–101, https://doi.org/10.1007/s40089-014-0124-5.

[70] S. Liu, W. Wang, Y. Cheng, L. Yao, H. Han, T. Zhu, Y. Liang, J. Fu, Methyl orange adsorption from aqueous solutions on 3D hierarchical PbS/ZnO microspheres, J. Colloid Interface Sci. 574 (2020) 410–420, https://doi.org/10.1016/j.jcis.2020.04.057.

[71] S. Wong, H.H. Tumari, N. Ngadi, N.B. Mohamed, O. Hassan, R. Mat, N.A. Saidina Amin, Adsorption of anionic dyes on spent tea leaves modified with polyethyleneimine (PEI-STL), J. Clean. Prod. 206 (2019) 394–406. doi:10.1016/j.jclepro.2018.09.201.

[72] W. Song, B. Gao, X. Xu, L. Xing, S. Han, P. Duan, W. Song, R. Jia, Adsorption-desorption behavior of magnetic amine/Fe3O4 functionalized biopolymer resin towards anionic dyes from wastewater, Bioresour. Technol. 210 (2016) 123–130, https://doi.org/10.1016/j.biortech.2016.01.078.

[73] B. Chen, S. Chen, H. Zhao, Y. Liu, F. Long, X. Pan, A versatile B-cyclodextrin and polyethyleneimine bi-functionalized magnetic nanoadsorbent for simultaneous capture of methyl orange and Pb(II) from complex wastewater, Chemosphere 216 (2019) 605–616, https://doi.org/10.1016/j.chemosphere.2018.10.157.

[74] Ş.S. Bayazit, Magnetic Multi-Wall Carbon Nanotubes for Methyl Orange Removal from Aqueous Solutions: Equilibrium, Kinetic and Thermodynamic Studies, Sep. Sci. Technol. 49 (2014) 1389–1400, https://doi.org/10.1080/01496395.2013.879595.

[75] Y.Z. Ma, D.F. Zheng, Z.Y. Mo, R.J. Dong, X.Q. Qiu, Magnetic lignin-based carbon nanoparticles and the adsorption for removal of methyl orange, Colloids Surfaces A Physicochem. Eng. Asp. 559 (2018) 226–234, https://doi.org/10.1016/j.colsurfa.2018.09.054.

[76] X. Ye, L. Wu, M. Zhu, Z. Wang, Z.H. Huang, M.X. Wang, Lotus pollen-derived hierarchically porous carbons with exceptional adsorption performance toward Reactive Black 5: Isotherms, kinetics and thermodynamics investigations, Sep. Purif. Technol. 300 (2022), 121899, https://doi.org/10.1016/j.seppur.2022.121899.

[77] A. Maleki, M. Mohammad, Z. Emdadi, N. Asim, M. Azizi, J. Safaei, Adsorbent materials based on a geopolymer paste for dye removal from aqueous solutions, Arab. J. Chem. 13 (2020) 3017–3025, https://doi.org/10.1016/j.arabjc.2018.08.011.

[78] T.A. Aragaw, A.N. Alene, A comparative study of acidic, basic, and reactive dyes adsorption from aqueous solution onto kaolin adsorbent: Effect of operating parameters, isotherms, kinetics, and thermodynamics, Emerg. Contam. 8 (2022) 59–74, https://doi.org/10.1016/j.emcon.2022.01.002.

[79] D.D. Eslek Koyuncu, M. Okur, Removal of AV 90 dye using ordered mesoporous carbon materials prepared via nanocasting of KIT-6: Adsorption isotherms, kinetics and thermodynamic analysis, Sep. Purif. Technol. 257 (2021) 117657. doi:10.1016/j.seppur.2020.117657.

[80] F.M. Teshager, N.G. Habtu, K. Mequanint, A systematic study of cellulose-reactive anionic dye removal using a sustainable bioadsorbent, Chemosphere 303 (2022), 135024, https://doi.org/10.1016/j.chemosphere.2022.135024.

[81] Y.A.B. Neolaka, Y. Lawa, J. Naat, A.A.P. Riwu, A.W. Mango, H. Darmokoesoemo, B. A. Widyaningrum, M. Iqbal, H.S. Kusuma, Efficiency of activated natural zeolite-based magnetic composite (ANZ-Fe_3O_4) as a novel adsorbent for removal of Cr(VI) from wastewater, J. Mater. Res. Technol. 18 (2022) 2896–2909, https://doi.org/10.1016/j.jmrt.2022.03.153.